

# Symmetric channel verification for purifying noisy quantum channels

Kento Tsubouchi,<sup>1,\*</sup> Yosuke Mitsuhashi,<sup>2</sup> Ryuji Takagi,<sup>2</sup> and Nobuyuki Yoshioka<sup>3,†</sup>

<sup>1</sup>*Department of Applied Physics, University of Tokyo, 7-3-1 Hongo, Bunkyo-ku, Tokyo 113-8656, Japan*

<sup>2</sup>*Department of Basic Science, University of Tokyo, 3-8-1 Komaba, Meguro-ku, Tokyo 153-8902, Japan*

<sup>3</sup>*International Center for Elementary Particle Physics, The University of Tokyo, 7-3-1 Hongo, Bunkyo-ku, Tokyo 113-0033, Japan*

Symmetry inherent in quantum states has been widely used to reduce the effect of noise in quantum error correction and a quantum error mitigation technique known as symmetry verification. However, these symmetry-based techniques exploit symmetry in quantum *states* rather than quantum *channels*, limiting their application to cases where the entire circuit shares the same symmetry. In this work, we propose symmetric channel verification (SCV), a channel purification protocol that leverages the symmetry inherent in quantum channels. By introducing different phases to each symmetric subspace and employing a quantum phase estimation-like circuit, SCV can detect and correct symmetry-breaking noise in quantum channels. We further propose a hardware-efficient implementation of SCV at the virtual level, which requires only a single-qubit ancilla and is robust against the noise in the ancilla qubit. Our protocol is applied to various Hamiltonian simulation circuits and phase estimation circuits, resulting in a significant reduction of errors. Furthermore, in setups where only Clifford unitaries can be used for noise purification, which is relevant in the early fault-tolerant regime, we show that SCV under Pauli symmetry represents the optimal purification method.

## I. INTRODUCTION

Protecting quantum computers from the effects of noise is one of the central challenges in the field of quantum computation. To achieve this goal, the symmetry inherent in quantum states has emerged as a powerful tool in reducing the effect of unwanted noise. For example, quantum error correction [1–10] detects and corrects errors by encoding logical quantum states into a symmetric subspace of the entire Hilbert space of physical qubits. Moreover, the quantum error mitigation [11–14] technique known as symmetry verification [15, 16] leverages problem-specific symmetry to filter out the effects of symmetry-breaking noise.

Despite their effectiveness, these symmetry-based protocols are primarily designed to exploit symmetry in quantum *states* rather than quantum *channels*. Therefore, for these methods to be applicable, the entire quantum circuit, including the input state, needs to share the same symmetry structure. In other words, symmetry-based protocols become ineffective when the input states or individual channels in the quantum circuit exhibit varying symmetries. To overcome these difficulties, we need to generalize the symmetry-based protocols to the channel level. One possible generalization is to utilize symmetry in channel purification protocols [17–19], where the noisy channel itself is purified by coherently connecting the input and output of the noisy quantum channel. However, the main focus of such protocols has been limited to utilizing Pauli symmetry for purifying near-Clifford circuits [20–25], while a comprehensive analysis of general channels and symmetries remains an open problem.

In this work, we bridge this gap by proposing *symmetric channel verification* (SCV). SCV is a novel channel purification protocol applicable to arbitrary symmetry inherent in quantum channels, and thus extends various notions of error countermeasures, such as error detection, virtual detection and error correction, to channel level (see Table I). Concretely, SCV detects symmetry-breaking noise in noisy channels by adding different phases to each symmetric subspace and using a quantum phase estimation-like circuit. We characterize the sufficient conditions for the noise to be completely removed by applying SCV. We also demonstrate that we can correct errors with no sampling overhead by applying feedback operations according to the detected errors. Moreover, we propose *virtual symmetric channel verification* (virtual SCV), a hardware-efficient implementation of SCV at the expectation value level. Virtual SCV can virtually detect symmetry-breaking noise using only a single qubit ancilla and is robust against noise affecting the ancilla. This method can be regarded as an extension of the virtual implementation of symmetry verification [26–29] to the channel level. Because of its robustness against the noise in ancilla qubit, virtual SCV can be used to completely mitigate errors on idling qubits, which appears frequently in early fault-tolerant algorithm based on qubitization [30–33].

As an application of our protocols, we apply SCV and virtual SCV under Pauli symmetry to mitigate logical errors on various early fault-tolerant quantum algorithms, such as Hamiltonian simulation and phase estimation. We demonstrate for certain well-structured Hamiltonian simulation circuits that, by applying SCV at the logical level, arbitrary single-qubit errors on the circuit can be detected and corrected. Moreover, we demonstrate that the effect of errors on idling qubits can be completely removed by virtual SCV. This is particularly useful in Hamiltonian simulation and phase estimation based on

\* tsubouchi@noneq.t.u-tokyo.ac.jp

† nyoshioka@ap.t.u-tokyo.ac.jp

	Error detection	Virtual detection	Error correction
State-level protocols	Refs. [15, 16]	Refs. [26–29]	Refs. [1–10]
Channel-level protocols	✓(SCV, Sec. III)	✓(Virtual SCV, Sec. IV)	✓(SCV+feedback, Sec. V)

TABLE I. Summary of the contributions of this work. In this work, we expand the error detection, virtual error detection, and error correction techniques for quantum *states* to quantum *channels*. More specifically, we introduce channel purification protocols that can detect (symmetric channel verification, SCV), virtually detect (virtual symmetric channel verification, virtual SCV), and correct (SCV + feedback) symmetry-breaking errors happening on quantum channels. Furthermore, in setups where only Clifford unitaries can be used for noise purification, relevant in the early fault-tolerant regime, we show that symmetric channel verification under Pauli symmetry represents the optimal protocol for detecting and correcting errors (Sec. VI).

qubitization, where we observe a quadratic reduction of logical errors. We also discuss applying SCV to quantum channels under particle number conservation symmetry.

We further discuss the ability of our protocols to purify noisy logical channels in the early fault-tolerant regime. When mitigating logical errors in this regime, it is desirable to implement Clifford unitaries [34–37], as they are relatively easy to implement at the logical level. Therefore, understanding the fundamental limitations in purifying noisy logical channels using Clifford unitaries is important from a practical perspective. Here, we show that for Hamiltonian simulation circuits, the noise detectable and correctable using channel purification protocols restricted to Clifford unitaries exactly matches the noise detectable and correctable using SCV under Pauli symmetry. Moreover, based on a resource-theoretic analysis [38], we derive an optimal bound for approximately purifying noisy Pauli rotation gates, where equality can be achieved using SCV under Pauli symmetry. These are remarkable examples of SCV fully exploiting the available operations to their ultimate limit.

By proposing SCV and virtual SCV, we provide a unified framework of channel purification protocols utilizing symmetries inherent in quantum channels. Thus, our results pave new ways for reducing errors in quantum computation. Moreover, SCV and virtual SCV offer various advantages over existing noise-reduction protocols. Unlike traditional symmetry verification methods [15, 16] and their virtual variants [26–29], which are state-level protocols, our channel-level protocols can be applied even when input states lack the requisite symmetry or when different quantum channels in a circuit exhibit varying symmetries. Compared to other channel purification protocols that require multiple noisy channels as input [17–19], symmetric channel verification requires only a single input, making it easier to implement in real devices. Furthermore, existing channel purification protocols that require a single noisy channel as input [20–24] can only purify noisy near-Clifford gates, whereas our method can be applied to general non-Clifford unitaries, regardless of whether the symmetry is discrete or continuous, Abelian or non-Abelian. Such fundamental distinctions highlight the advancement achieved in our work.

This paper is organized as follows. In Sec. II, we introduce the setup of channel purification. Sec. III focuses on symmetric channel verification (SCV), providing theoretical details and implementation strategies. Sec. IV

presents virtual symmetric channel verification (virtual SCV), a hardware-efficient variant of SCV. In Sec. V, we consider correcting errors rather than detecting them using SCV. Finally, Sec. VI discusses the limitations of channel purification protocols restricted to Clifford unitaries. We make our conclusion in Sec. VII by summarizing our results and discussing possible future directions.

## II. SETUP OF CHANNEL PURIFICATION

We first provide the problem setup considered in the task of channel purification [17–24]. Let us assume that we want to implement an  $n$ -qubit unitary channel  $\mathcal{U}(\cdot) = U \cdot U^\dagger$ , but the channel is affected by a noise channel  $\mathcal{N}$ . As depicted in Fig. 1 (a), channel purification aims to eliminate the effect of noise channel  $\mathcal{N}$  under the constraint that we only have access to the noisy channel  $\mathcal{U}_{\mathcal{N}}$ , by coherently connecting the input and output of the noisy channel with ancilla qubits. Concretely, we prepare  $m$ -qubit ancilla initialized in  $|0^m\rangle$  and apply  $(n+m)$ -qubit unitary operations  $\mathcal{U}_{\text{E}}(\cdot) = U_{\text{E}} \cdot U_{\text{E}}^\dagger$  and  $\mathcal{U}_{\text{D}}(\cdot) = U_{\text{D}} \cdot U_{\text{D}}^\dagger$  before and after the noisy channel  $\mathcal{U}_{\mathcal{N}}$ . Then, we measure the ancilla qubits in the computational basis and either (i) post-select, (ii) average, or (iii) discard the measurement results. In the following, let us describe how these processes can be understood as transforming the noisy channel  $\mathcal{U}_{\mathcal{N}}$  using a quantum supermap  $\Theta$ .

First, post-selecting the measurement results corresponds to transforming the noisy channel  $\mathcal{U}_{\mathcal{N}}$  into a trace non-increasing map  $\Theta^{\text{det}}(\mathcal{U}_{\mathcal{N}})$  defined as

$$\rho \mapsto \langle 0^m | \mathcal{U}_{\text{D}} \circ (\mathcal{U}_{\mathcal{N}} \otimes \mathcal{I}_{\text{a}}) \circ \mathcal{U}_{\text{E}}(\rho \otimes |0^m\rangle\langle 0^m|) | 0^m \rangle. \quad (1)$$

This map outputs the normalized quantum state with probability  $\text{tr}[(\Theta^{\text{det}}(\mathcal{U}_{\mathcal{N}}))(\rho)]$ . Here,  $|0^m\rangle$  represents the initial state in the ancilla qubits and  $\mathcal{I}_{\text{a}}$  is the identity operation on the ancilla qubits. Channel purification with post-selection can be regarded as detecting errors in the noise channel  $\mathcal{N}$ . In Sec. III, we propose channel purification protocol that can detect symmetry-breaking errors by appropriately constructing the unitaries  $U_{\text{E}}$  and  $U_{\text{D}}$  in this setup.

Second, when we average the measurement results, the effect of the transformed channel can be regarded as a

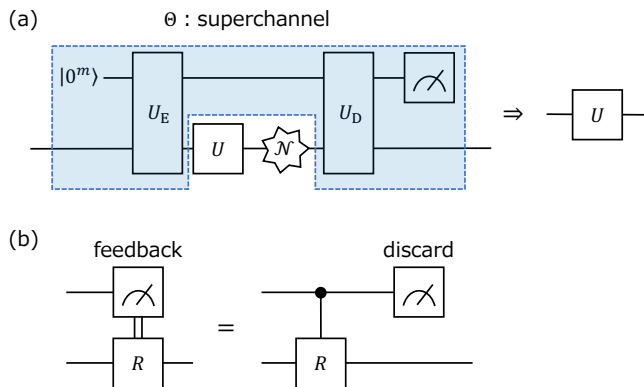


FIG. 1. Schematic of channel purification. (a) We aim to reduce the effect of the noise  $\mathcal{N}$  by preparing  $m$ -qubit ancilla initialized in  $|0^m\rangle$ , applying  $(n+m)$ -qubit unitary operations  $U_E$  and  $U_D$  before and after the noisy channel, and measuring the ancilla qubits in the computational basis either to (i) post-select, (ii) average, or (iii) discard the measurement results. These operations can be regarded as applying a quantum supermap  $\Theta$  to the noisy channel. (b) Applying feedback control to the system can be interpreted as applying control operation and discarding the measurement results.

virtual map  $\Theta^{\text{vir}}(\mathcal{U}_{\mathcal{N}})$  acting as

$$\rho \mapsto \text{tr}_a[\mathcal{U}_D \circ (\mathcal{U}_{\mathcal{N}} \otimes \mathcal{I}_a) \circ \mathcal{U}_E(\rho \otimes |0^m\rangle\langle 0^m|)(I_n \otimes Z^{\otimes m})], \quad (2)$$

where  $I_n$  is the identity operator of the  $n$ -qubit system. Here, a virtual map means that we cannot obtain the output quantum state  $(\Theta^{\text{vir}}(\mathcal{U}_{\mathcal{N}}))(\rho)$  itself, but it can only be used to calculate an expectation value of an observable  $O$  as  $\text{tr}[(\Theta^{\text{vir}}(\mathcal{U}_{\mathcal{N}}))(\rho)O]$ . In Sec. IV, we propose a virtual error detection protocol that can simulate the error-detected map  $\Theta^{\text{det}}(\mathcal{U}_{\mathcal{N}})$  using virtual map  $\Theta^{\text{vir}}(\mathcal{U}_{\mathcal{N}})$  with smaller hardware overhead.

Finally, discarding the measurement results leads to applying a superchannel  $\Theta^{\text{cor}}$  which maps the noisy channel  $\mathcal{U}_{\mathcal{N}}$  into a valid quantum channel  $\Theta^{\text{cor}}(\mathcal{U}_{\mathcal{N}})$  defined as

$$\rho \mapsto \text{tr}_a[\mathcal{U}_D \circ (\mathcal{U}_{\mathcal{N}} \otimes \mathcal{I}_a) \circ \mathcal{U}_E(\rho \otimes |0^m\rangle\langle 0^m|)]. \quad (3)$$

We note that measuring the ancilla qubits and applying feedback control to the system can be characterized using  $\Theta^{\text{cor}}$  by replacing the measurement+feedback control with controlled-unitary before the measurement (see Fig. 1 (b)). Therefore, channel purification discarding the measurement results corresponds to correcting errors in the noise channel  $\mathcal{N}$ . In Sec. V, we construct a channel purification protocol that can correct symmetry-breaking errors in this setup.

Note that  $U_E$  and  $U_D$  themselves are noisy in practice, and hence we wish them to be as simple as possible. Therefore, in the early fault-tolerant regime, where Clifford gates can be implemented straightforwardly in many quantum error correction codes, we wish them to be Clifford unitaries from a practical perspective. We discuss

the limitations of channel purification protocols under such restriction in Sec. VI. Throughout our work, our theoretical analysis assumes noiseless  $U_E$  and  $U_D$ , while we numerically investigate the performance under noisy  $U_E$  and  $U_D$ .

### III. SYMMETRIC CHANNEL VERIFICATION

#### A. General framework

In many quantum circuits, the unitary  $U$  we aim to implement often exhibits inherent symmetry. We assume that we know an operator  $S$  such that  $[U, S] = 0$ ; for instance, when considering the time evolution of a Hamiltonian  $H$  with particle number conservation symmetry,  $U = e^{i\theta H}$  commutes with  $S = \sum_i Z_i$ . Additionally, when  $U$  is part of a quantum circuit that can be diagonalized in the computational basis, we have  $[U, S] = 0$  with  $S = Z_i$ . In these cases,  $U$  can be block-diagonalized with respect to the eigenspaces of  $S$ . Let  $\{\Pi_i\}_{i=1}^M$  represent the set of projectors onto the eigenspaces of  $S$ . The ideal unitary  $U$  can then be expressed as  $U = \sum_i \Pi_i U \Pi_i$ , representing its block diagonalization. Thus, the ideal channel  $\mathcal{U}$  can be decomposed as

$$\mathcal{U}(\cdot) = \sum_{i,j} \Pi_i \mathcal{U}(\Pi_i \cdot \Pi_j) \Pi_j, \quad (4)$$

indicating that  $\mathcal{U}$  maps the  $(i, j)$ -th block element to the  $(i, j)$ -th block element.

When the input state  $\rho$  to the unitary  $U$  lies within an eigenspace of  $S$  as  $\rho = \Pi_i \rho \Pi_i$ , the ideal output state also remains in the eigenspace as  $\mathcal{U}(\rho) = \Pi_i \mathcal{U}(\rho) \Pi_i$ . This property can be utilized to detect noise  $\mathcal{N}$  that breaks the symmetry by using a quantum error mitigation technique called symmetry verification [15, 16]. By measuring the noisy state  $\mathcal{U}_{\mathcal{N}}$  with the POVM  $\{\Pi_i\}_{i=1}^M$  and post-selecting  $\Pi_i$ , symmetry verification detects symmetry-breaking errors and produces a state

$$\frac{\Pi_i \mathcal{U}_{\mathcal{N}}(\rho) \Pi_i}{\text{tr}[\Pi_i \mathcal{U}_{\mathcal{N}}(\rho) \Pi_i]} \quad (5)$$

with probability  $\text{tr}[\Pi_i \mathcal{U}_{\mathcal{N}}(\rho) \Pi_i]$ . This state has a larger overlap with the ideal state  $\mathcal{U}(\rho)$  compared to the noisy state  $\mathcal{U}_{\mathcal{N}}(\rho)$ , so the impact of noise is effectively reduced.

Conversely, if the input state  $\rho$  does not lie within an eigenspace of  $S$ , the ideal output state  $\mathcal{U}(\rho)$  will also not belong to an eigenspace of  $S$ . In such cases, symmetry verification cannot be applied to detect noise  $\mathcal{N}$ , as the measurement with the POVM  $\{\Pi_i\}_{i=1}^M$  may disrupt the ideal state  $\mathcal{U}(\rho)$ . These scenarios frequently arise when one wishes to simulate time evolution of either time-independent or dependent Hamiltonian for arbitrary states, or when  $U$  is a component of a quantum circuit where other parts lack the same symmetry. Nevertheless, the noise  $\mathcal{N}$  still breaks the symmetry of the ideal channel  $\mathcal{U}$ , preventing the  $(i, j)$ -th block element

from being mapped to the  $(i, j)$ -th block element as described in Eq. (4). This symmetry-breaking property can be exploited to reduce noise effects by purifying the noisy channel  $\mathcal{U}_{\mathcal{N}}$  itself, rather than the output state  $\mathcal{U}_{\mathcal{N}}(\rho)$ .

Here, we propose *symmetric channel verification* (SCV), a channel purification protocol that purifies the noisy channel  $\mathcal{U}_{\mathcal{N}}(\cdot)$  by detecting symmetry-breaking noise. To implement SCV, we utilize the circuit structure depicted in Fig. 2. The SCV gadget introduces different phases to each symmetric subspace and employs a quantum phase estimation-like circuit to detect changes in the symmetric subspace before and after the noisy channel. We first prepare  $m = \lceil \log_2 M \rceil$ -qubit ancilla and apply a Hadamard gate to each ancilla qubit. Next, for  $k = 1, \dots, m$ , we sandwich the noisy channel  $\mathcal{U}_{\mathcal{N}}$  between controlled- $V_S^{2^{k-1}}$  and controlled- $V_S^{\dagger 2^{k-1}}$ , where  $k$ -th ancilla qubit is taken as the control qubit and  $V_S$  applies a phase  $\exp\left[\frac{2\pi i}{2^m} j\right]$  to the  $j$ -th eigenspace as

$$V_S = \sum_j \exp\left[\frac{2\pi i}{2^m} j\right] \Pi_j. \quad (6)$$

Then, the inverse quantum Fourier transform is applied to the ancilla. Finally, we measure the ancilla in the computational basis and post-select the measurement result  $|0^m\rangle$ .

When a state  $\rho$  is an input to this circuit, the state before measurement is

$$\frac{1}{2^m} \sum_{i'j'jkk'} \delta_{i,i'+k} \delta_{j,j'+k'} \Pi_{i'} \mathcal{U}_{\mathcal{N}}(\Pi_i \rho \Pi_j) \Pi_{j'} \otimes |k\rangle\langle k'|, \quad (7)$$

where  $\delta$  represents the Kronecker delta with mod  $2^m$ . Upon post-selection with  $|0^m\rangle$ , the resulting state becomes

$$\frac{\sum_{ij} \Pi_i \mathcal{U}_{\mathcal{N}}(\Pi_i \rho \Pi_j) \Pi_j}{\text{tr}[\sum_{ij} \Pi_i \mathcal{U}_{\mathcal{N}}(\Pi_i \rho \Pi_j) \Pi_j]} \quad (8)$$

with probability  $\text{tr}[\sum_{ij} \Pi_i \mathcal{U}_{\mathcal{N}}(\Pi_i \rho \Pi_j) \Pi_j]$ . Thus, SCV maps the noisy channel  $\mathcal{U}_{\mathcal{N}}$  to a trace non-increasing map  $(\Theta_S^{\text{det}}(\mathcal{U}_{\mathcal{N}}))(\cdot) = \sum_{ij} \Pi_i \mathcal{U}_{\mathcal{N}}(\Pi_i \cdot \Pi_j) \Pi_j$ .

Through this channel transformation, the effects of symmetry-breaking noise are removed. To illustrate, consider a noise channel expressed as  $\mathcal{N}(\cdot) = (1-p) \cdot + p \sum_j N_j \cdot N_j^\dagger$  with  $\sum_i \Pi_i N_j \Pi_i = 0$ , indicating that with probability  $p$ , a quantum state in the  $i$ -th eigenspace transitions outside the eigenspace. In this scenario,  $\Theta_S^{\text{det}}(\mathcal{U}_{\mathcal{N}}) = (1-p)\mathcal{U}$ , meaning the noise effect is removed with probability  $1-p$ . More generally, we establish the following theorem:

**Theorem 1.** Let  $\Theta_S^{\text{det}}$  denote a quantum supermap as defined in Fig. 2. If the noise channel  $\mathcal{N}(\cdot) = \sum_j N_j \cdot N_j^\dagger$  satisfies  $\sum_i \Pi_i N_j \Pi_i \propto I_n$ , then

$$(\Theta_S^{\text{det}}(\mathcal{U}_{\mathcal{N}}))(\cdot) = \sum_{ij} \Pi_i \mathcal{U}_{\mathcal{N}}(\Pi_i \cdot \Pi_j) \Pi_j \propto \mathcal{U}(\cdot). \quad (9)$$

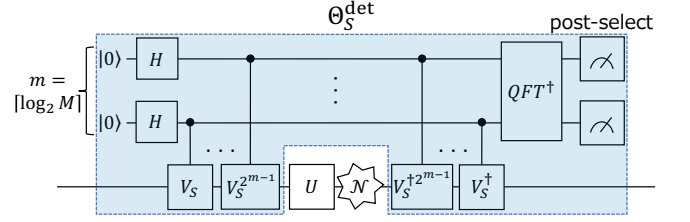


FIG. 2. Circuit structure of symmetric channel verification (SCV). We prepare  $m = \lceil \log_2 M \rceil$ -qubit ancilla, apply Hadamard gate, apply controlled- $V_S^{2^{k-1}}$  for  $k = 1, \dots, m$  where the  $k$ -th ancilla is the control qubit and  $V_S = \sum_j \exp\left[\frac{2\pi i}{2^m} j\right] \Pi_j$ , apply the noisy channel  $\mathcal{U}_{\mathcal{N}} = \mathcal{N} \circ \mathcal{U}$ , apply controlled- $V_S^{\dagger 2^{k-1}}$  for  $k = 1, \dots, m$ , perform the inverse quantum Fourier transform, measure the ancilla qubits in the computational basis, and post-select the measurement result  $|0^m\rangle$ . This operation transforms the noisy channel  $\mathcal{U}_{\mathcal{N}}(\cdot)$  into  $(\Theta_S^{\text{det}}(\mathcal{U}_{\mathcal{N}}))(\cdot) = \sum_{ij} \Pi_i \mathcal{U}_{\mathcal{N}}(\Pi_i \cdot \Pi_j) \Pi_j$ .

Consequently, when a state  $\rho$  is input to the circuit in Fig. 2, the ideal output state  $\mathcal{U}(\rho)$  is obtained with probability  $\text{tr}[\sum_{ij} \Pi_i \mathcal{U}_{\mathcal{N}}(\Pi_i \rho \Pi_j) \Pi_j]$ .

SCV can be seen as a generalization of symmetry verification to the channel level. Indeed, we can detect the effects of symmetry-breaking noise, regardless of the input state. Furthermore, SCV can detect symmetry-breaking noise occurring during the execution of  $\mathcal{U}$ . For simplicity, let us assume that  $\mathcal{U} = \mathcal{U}_2 \circ \mathcal{U}_1$  is implemented by performing two consecutive unitary channels  $\mathcal{U}_1(\cdot) = U_1 \cdot U_1^\dagger$  and  $\mathcal{U}_2(\cdot) = U_2 \cdot U_2^\dagger$ , with the noise channel  $\mathcal{N}$  occurring between  $\mathcal{U}_1$  and  $\mathcal{U}_2$  as  $\mathcal{U}_2 \circ \mathcal{N} \circ \mathcal{U}_1$ . Even in this case, if  $U_1$  and  $U_2$  both commute with the operator  $S$  and the noise  $\mathcal{N}$  satisfies the assumption in Theorem 1, the SCV gadget can completely eliminate the noise as  $\Theta_S^{\text{det}}(\mathcal{U}_2 \circ \mathcal{N} \circ \mathcal{U}_1) \propto \mathcal{U}_2 \circ \mathcal{U}_1 = \mathcal{U}$ . This demonstrates that SCV can purify arbitrary symmetry-breaking noise occurring during circuit execution.

If the ideal unitary  $U$  has multiple commuting operators, we can concatenate the SCV gadget for different symmetries to further purify the noisy channel. For example, in addition to  $S$ , if the unitary operator  $U$  also commutes with another operator  $S'$ , which has the set of projectors  $\{\Pi'_i\}_{i=1}^{M'}$  onto its eigenspaces, the ideal channel satisfies  $\mathcal{U}(\cdot) = \sum_{ijkl} \Pi'_i \Pi_j \mathcal{U}(\Pi_j \Pi'_i \cdot \Pi'_k \Pi_l) \Pi_l \Pi'_k$ . Therefore, by concatenating the SCV gadget for the symmetric operators  $S$  and  $S'$ , we obtain a purified channel

$$(\Theta_{S'}^{\text{det}} * \Theta_S^{\text{det}}(\mathcal{U}_{\mathcal{N}}))(\cdot) = \sum_{ijkl} \Pi'_i \Pi_j \mathcal{U}_{\mathcal{N}}(\Pi_j \Pi'_i \cdot \Pi'_k \Pi_l) \Pi_l \Pi'_k. \quad (10)$$

Here, the composition of supermaps is defined as  $\Theta_{S'}^{\text{det}} * \Theta_S^{\text{det}}(\cdot) = \Theta_{S'}^{\text{det}}(\Theta_S^{\text{det}}(\cdot))$ . This channel is proportional to the ideal channel  $\mathcal{U}$  when the noise channel  $\mathcal{N}(\cdot) = \sum_k N_k \cdot N_k^\dagger$  satisfies  $\sum_{ij} \Pi'_j \Pi_i N_k \Pi_i \Pi'_j \propto I_n$ . This condition is less restrictive than the assumption in Theorem 1: it is satisfied when  $N_k$  breaks the symmetry with respect

to either  $S$  or  $S'$ . Therefore, we can purify a broader range of noise by concatenating SCV gadgets for different symmetries.

Let us comment on the implementation overhead of SCV. Implementing SCV requires controlled- $V_S$  gates and a quantum Fourier transform, which may necessitate many quantum gates and introduce additional noise into the circuit. However, the hardware overhead for SCV does not depend on the depth of the target unitary. Therefore, when the unitary  $U$  is sufficiently deep and contains significantly more quantum gates, the dominant noise in the circuit will be the noise  $\mathcal{N}$  following the unitary  $U$ . In this case, the noise introduced during SCV becomes negligible, and the overall effect of noise can be reliably reduced. In the case where the noise affecting the SCV gadget is prohibitively large, we can use the hardware-efficient variant of SCV we introduce in Sec. IV.

Another type of overhead associated with SCV is sampling overhead. Namely, the number of circuit runs required to obtain the desired results with target accuracy is increased, because we obtain the purified channel probabilistically. For example, when the noise can be expressed as  $\mathcal{N}(\cdot) = (1-p) \cdot \text{id} + p \sum_j N_j \cdot N_j^\dagger$  with  $\sum_i \Pi_i N_j \Pi_i = 0$ , we obtain the noiseless purified channel with probability  $1-p$ . Therefore, we need approximately  $(1-p)^{-1} \sim (1+p)$  times as many circuit runs as in the noiseless case. Furthermore, when there are  $L$  noisy channels  $\mathcal{U}_{\mathcal{N}}$  and SCV is applied to each channel, the sampling overhead scales as  $O((1+p)^L)$ . Notably, this is quadratically smaller than the lower bound on sampling overhead for quantum error mitigation, which scales as  $O((1+p)^{2L})$  [39, 40]. This improvement arises because SCV allows coherent interaction between the system and the ancilla before and after the noisy gate, a feature not considered in theoretical analyses of quantum error mitigation [39–42].

## B. Application to Pauli symmetry

As an application of SCV, let us consider a quantum channel under Pauli symmetry, which is present in various quantum algorithms including quantum many-body simulation, quantum machine learning, and quantum information processing. Here, we first derive a general condition to completely eliminate the effect of noise, and then later provide numerical demonstrations for practical quantum circuits.

Let us define the set of  $n$ -qubit Pauli operators as  $\mathcal{P}_n = \{I, X, Y, Z\}^{\otimes n}$ . Here,  $I$  represents the identity operator on a single-qubit system, which we distinguish from the  $n$ -qubit identity operator  $I_n$ . For simplicity, let us analyze the case where the noise channel  $\mathcal{N}$  is Pauli noise represented as

$$\mathcal{N}(\cdot) = \sum_{i=0}^K p_i P_i \cdot P_i, \quad (11)$$

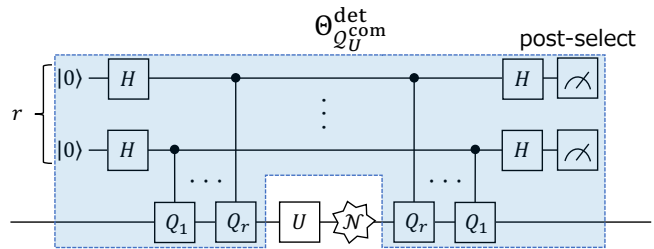


FIG. 3. Circuit structure of SCV for the set of Pauli operators  $\mathcal{Q}_U^{\text{com}}$ . We concatenate the SCV gadget for the generator  $Q_1, \dots, Q_r \in \mathcal{Q}_U^{\text{com}}$  as  $\Theta_{\mathcal{Q}_U^{\text{com}}}^{\text{det}} = \Theta_{Q_1}^{\text{det}} * \dots * \Theta_{Q_r}^{\text{det}}$ .

where  $p_i \neq 0$  denotes the probability of an  $n$ -qubit Pauli operator  $P_i \in \mathcal{P}_n$  affecting the target unitary,  $P_0 = I_n$  represents the  $n$ -qubit identity operator, and  $P_i \neq P_j$  if  $i \neq j$ . Although our discussion assumes Pauli noise, it can be generalized to arbitrary noise by decomposing the Kraus operators into the sum of Pauli operators.

First, we consider the simplest case where the ideal unitary operator  $U$  commutes with a single nontrivial Pauli operator  $Q \in \mathcal{P}_n \setminus \{I_n\}$ , i.e.,  $[U, Q] = 0$ . The Pauli operator  $Q$  has two eigenspaces with projectors  $\Pi_0 = \frac{1}{2}(I + Q)$  and  $\Pi_1 = \frac{1}{2}(I - Q)$ . In this scenario, the operator  $V_Q$  defined in Eq. (6) is the Pauli operator  $Q$  itself. Therefore, implementing SCV requires only a single-qubit ancilla and two controlled- $Q$  gates. By performing SCV, we can detect Pauli error  $P_j \in \mathcal{P}_n \setminus \{I_n\}$  satisfying  $\sum_i \Pi_i P_j \Pi_i \propto I_n$ , i.e., Pauli error  $P_j$  that anti-commute with  $Q$ .

Next, we consider the case where the ideal unitary operator  $U$  commutes with multiple nontrivial Pauli operators. As we have discussed, SCV gadgets can be concatenated for different commuting Pauli operators. To formalize this analysis, we define the set of Pauli operators with non-zero coefficients in the Pauli expansion of  $U$  as

$$\mathcal{Q}'_U = \{Q \in \mathcal{P}_n \mid \text{tr}[UQ] \neq 0\}, \quad (12)$$

the set of Pauli operators generated by  $\mathcal{Q}'_U$  up to phase as

$$\mathcal{Q}_U = \{Q \in \mathcal{P}_n \mid \exists Q_{i_1}, \dots, Q_{i_j} \in \mathcal{Q}'_U, Q \propto Q_{i_1} \dots Q_{i_j}\}, \quad (13)$$

and the set of Pauli operators that commutes with  $U$  as

$$\mathcal{Q}_U^{\text{com}} = \{Q \in \mathcal{P}_n \mid [U, Q] = 0\}. \quad (14)$$

Let  $Q_1, \dots, Q_r \in \mathcal{Q}_U^{\text{com}}$  be generators of the set of Pauli operators  $\mathcal{Q}_U^{\text{com}}$  up to phase. As shown in Fig. 3, we concatenate the SCV gadget for  $Q_1, \dots, Q_r$  and define the SCV gadget for the set of commuting Pauli operators  $\mathcal{Q}_U^{\text{com}}$  as

$$\Theta_{\mathcal{Q}_U^{\text{com}}}^{\text{det}} = \Theta_{Q_1}^{\text{det}} * \dots * \Theta_{Q_r}^{\text{det}}. \quad (15)$$

Since  $\Theta_{Q_i}^{\text{det}}$  can detect Pauli errors that anti-commute with  $Q_i$ ,  $\Theta_{\mathcal{Q}_U^{\text{com}}}^{\text{det}}$  can detect Pauli errors that anti-commute with at least one of the generators. In other

words, the SCV gadget for  $\mathcal{Q}_U^{\text{com}}$  can detect a Pauli error  $P_j$  if there exists a Pauli operator  $Q \in \mathcal{Q}_U^{\text{com}}$  that anti-commutes with  $P_j$ . Thus, the performance of SCV for Pauli symmetry is characterized by the following corollary:

**Corollary 1.** For Pauli noise channel  $\mathcal{N}(\cdot) = \sum_{i=0}^K p_i P_i \cdot P_i$ , defined in Eq. (11), let  $\mathcal{P}_N^{\text{det}} = \{P_i\}_{i=1}^K$  denote the set of Pauli operators that yield nonzero error probability. Then, the SCV gadget  $\Theta_{\mathcal{Q}_U^{\text{com}}}^{\text{det}}$  for the set of commuting Pauli operators  $\mathcal{Q}_U^{\text{com}}$ , as defined in Fig. 3, can completely detect the Pauli noise  $\mathcal{N}$ , i.e.,  $\Theta_{\mathcal{Q}_U^{\text{com}}}^{\text{det}}(\mathcal{U}_N) = p_0 \mathcal{U}$ , if and only if all the Pauli error  $P_i \in \mathcal{P}_N^{\text{det}}$  anti-commutes with at least one of the  $Q_j \in \mathcal{Q}_U^{\text{com}}$ :

$$\forall P_i \in \mathcal{P}_N^{\text{det}}, \exists Q_j \in \mathcal{Q}_U^{\text{com}}, [P_i, Q_j] \neq 0, \quad (16)$$

or equivalently,

$$\mathcal{P}_N^{\text{det}} \cap \mathcal{Q}_U = \emptyset. \quad (17)$$

Corollary 1 states that the SCV gadget for the set of Pauli operators  $\mathcal{Q}_U$  can detect arbitrary Pauli errors that are not part of the ideal unitary  $U$ . In this case, a noiseless channel  $\mathcal{U}$  is obtained with probability  $p_0$ . However, the SCV gadget cannot detect Pauli errors contained within  $U$  because such errors share the same Pauli symmetry as  $U$  and commute with all elements in  $\mathcal{Q}_U^{\text{com}}$ .

To demonstrate the power of SCV for Pauli symmetry, we consider the time-independent and time-dependent Hamiltonian dynamics simulation. While state-level noise detection protocols [15, 16] can only be used when the entire circuit possesses the same symmetric structure, SCV can be applied even when the input state does not commute with the same Pauli operators or when the symmetric structure of the Hamiltonian changes over time. Let us first discuss the time-independent Hamiltonian simulation circuit  $U = e^{i\theta H}$ , where  $H$  represents the Hamiltonian of interest. Note that, while Trotter or post-Trotter circuits are implemented in practice, here we neglect the effect of imperfect exponentiation for the sake of demonstration of SCV. Under perfect exponentiation, we generally have  $\mathcal{Q}_U = \mathcal{Q}_H$  and  $\mathcal{Q}_U^{\text{com}} = \mathcal{Q}_H^{\text{com}}$ , and SCV can be applied regardless of the input state.

One interesting time-independent Hamiltonian to examine is the 1D Heisenberg model  $H = \sum_i (X_i X_{i+1} + Y_i Y_{i+1} + Z_i Z_{i+1})$ , whose dynamics simulation using quantum computer is an active topic of research [43, 44]. For this Hamiltonian, we have  $\mathcal{Q}_H^{\text{com}} = \{I^{\otimes n}, X^{\otimes n}, Y^{\otimes n}, Z^{\otimes n}\}$ . Since any weight-1 Pauli operator anti-commutes with  $X^{\otimes n}$  or  $Z^{\otimes n}$ , we can detect single-qubit Pauli errors occurring during the time evolution. Meanwhile, two-qubit Pauli errors such as  $XX$  commute with all the element in  $\mathcal{Q}_H^{\text{com}}$ , so such error cannot be detected. To numerically verify the effectiveness of SCV, we consider an  $n = 8$  qubit 1D Heisenberg model with an open boundary condition and apply the time

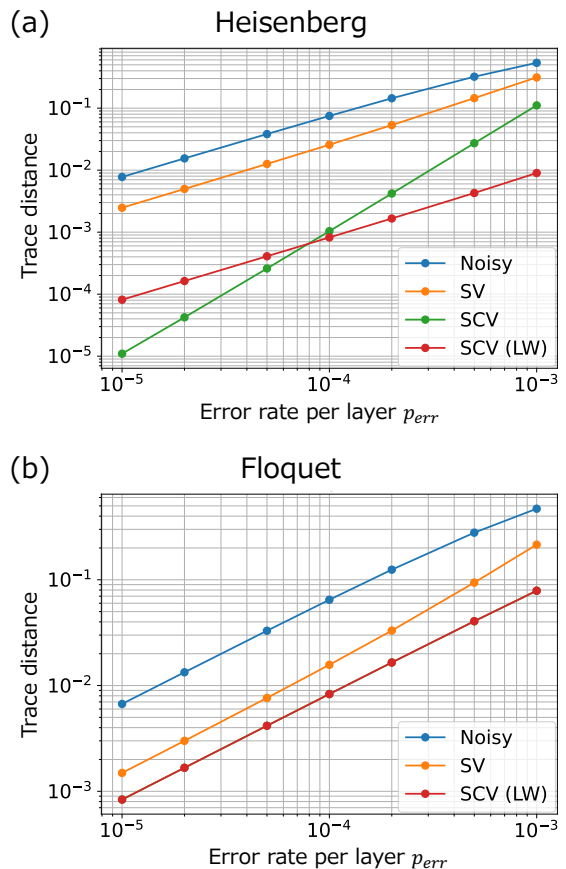


FIG. 4. Performance of SCV in detecting errors on Hamiltonian simulation circuits for (a) 1D Heisenberg model and (b) Floquet dynamics. The “Noisy” line represents the trace distance between the noisy quantum state and the ideal quantum state, while the “SV” line represents the trace distance for the quantum state purified by symmetry verification. The “SCV” line represents the trace distance where the SCV is applied to the entire noisy circuit  $\bigcirc_{i=1}^L \mathcal{N}_i \circ \mathcal{U}_i$ , and the “SCV (LW)” line represents the layer-wise application of SCV, meaning that SCV is applied to every noisy layer ( $\mathcal{N}_i \circ \mathcal{U}_i$  for (a) Heisenberg model and  $\mathcal{N}_i \circ \mathcal{U}_{X,i}$  and  $\mathcal{N}_i \circ \mathcal{U}_{Z,i}$  for (b) Floquet dynamics).

evolution  $U = e^{i\theta H}$  to the input state  $|01\rangle^{\otimes n/2}$ . We assume that the noisy circuit is represented as  $\bigcirc_{i=1}^L \mathcal{N}_i \circ \mathcal{U}_i$ , where  $\mathcal{N}_i$  is a local depolarizing noise with an error rate  $p_{\text{err}}$  and  $\mathcal{U}_i(\cdot) = e^{i(\theta/L)H} \cdot e^{-i(\theta/L)H}$  represents a single time step. We further assume that the controlled-Pauli gates composing the SCV gadget are also affected by local depolarizing noise with an error rate  $p_{\text{err}}/100$ . The difference in error rates arises because approximately 100 Clifford+T gates are required to synthesize Pauli rotation gates with an accuracy of  $10^{-6}$  [45]. We set  $\theta = 2\pi$  and  $L = 100$ .

Our results are illustrated in Fig. 4 (a). Since the input state  $|01\rangle^{\otimes n/2}$  is an eigenstate of the operator  $Z^{\otimes n}$ , we can apply symmetry verification for  $Z^{\otimes n}$  and detect arbitrary single-qubit bit-flip errors. However, it is not an eigenstate of the operator  $X^{\otimes n}$ , so symmetry verification

cannot be applied for  $X^{\otimes n}$ , even though the Hamiltonian commutes with  $X^{\otimes n}$ . Meanwhile, SCV does not depend on the input state, allowing us to detect arbitrary errors that anti-commute with  $X^{\otimes n}$  or  $Z^{\otimes n}$ . Thus, while symmetry verification reduces the error by a constant factor, SCV applied to the entire noisy circuit  $\bigcirc_{l=1}^L \mathcal{N}_l \circ \mathcal{U}_l$  can detect arbitrary single-qubit errors and quadratically reduce the error rate. Further error reduction can be achieved by applying SCV at every layer  $\mathcal{N}_l \circ \mathcal{U}_l$ . In this case, more errors can be detected during the time evolution, but the impact of errors on the SCV gadget itself becomes dominant. As a result, the scaling of the error worsens compared to applying SCV to the entire circuit, but in high-error-rate regimes, layerwise SCV application performs better.

Next, as an example of time-dependent Hamiltonian dynamics simulation, we consider the Floquet system [46], whose Hamiltonian changes time-periodically. Floquet systems exhibit a rich set of physical phenomena and thus have been widely simulated on quantum computers [47–49]. We consider a noiseless circuit represented as  $\bigcirc_{l=1}^L \mathcal{U}_{X,l} \circ \mathcal{U}_{Z,l}$ , where  $\mathcal{U}_{X,l}(\cdot) = e^{i\theta H_X} \cdot e^{-i\theta H_X}$  with  $H_X = \sum_i X_i$  and  $\mathcal{U}_{X,l}(\cdot) = e^{i\theta H_X} \cdot e^{-i\theta H_X}$  with  $H_Z = \sum_i Z_i Z_{i+1}$ . This represents that Hamiltonian changes time-periodically between  $H_X$  and  $H_Z$ . When we take  $|+\rangle^{\otimes n}$  as an input to this circuit, the output state is an eigenstate of the operator  $X^{\otimes n}$ , allowing us to perform symmetry verification for  $X^{\otimes n}$ . Meanwhile, each layer  $e^{i\theta H_X}$  and  $e^{i\theta H_Z}$  commutes with additional Pauli operators:  $\mathcal{Q}_{H_X}^{\text{com}} = \{I, X\}^{\otimes n}$  and  $\mathcal{Q}_{H_Z}^{\text{com}} = \{I, Z\}^{\otimes n} \cdot \{I_n, X^{\otimes n}\}$ . Therefore, by applying SCV to each layer, we can detect more errors compared to simply applying symmetry verification to the output state.

To evaluate the effectiveness of SCV in this scenario, we consider a noisy circuit  $\bigcirc_{l=1}^L \mathcal{N}_l \circ \mathcal{U}_{X,l} \circ \mathcal{N}_l \circ \mathcal{U}_{Z,l}$  with  $n = 4$ , where  $\mathcal{N}_l$  is a local depolarizing noise with an error rate  $p_{\text{err}}$ . We set  $\theta = 2\pi/100$  and  $L = 100$ . We further assume that the controlled-Pauli gates composing the SCV gadget are also affected by local depolarizing noise with an error rate  $p_{\text{err}}/100$ . As shown in Fig. 4 (b), even with noise in the SCV gadget, SCV can significantly reduce the effect of noise in the circuit.

Let us comment on the differences between our analysis of SCV under Pauli symmetry and previous works based on similar ideas. In Refs. [20–24], the authors introduce a purification gadget similar to the one shown in Fig. 3 to purify noisy near-Clifford circuits. The primary focus of these studies is on the case where  $U$  consists of Clifford gates. They proposed that, in this setting, arbitrary errors can be detected by sandwiching  $U$  with a controlled Pauli gate and its conjugate under  $U$ . Furthermore, they analyzed the case where  $U$  consists of Clifford gates supplemented with Pauli-Z rotation gates. In this scenario, they claimed that noisy Pauli-Z rotation gates can be purified by sandwiching them with controlled-Z gates, which is precisely what SCV for the Pauli-Z operator is doing. One of the main contributions of our work is to extend these analyses beyond simple Pauli rotation

gates to general non-Clifford channels  $U$ . As stated in Corollary 1 and discussed in Sec. VI, we establish the ultimate performance limits of such purification protocols.

### C. Application to particle number conservation symmetry

Symmetry arising from particle number conservation plays a crucial role in many quantum systems, especially in the context of fermionic systems. The particle number conservation symmetry is defined by the commutation of the Hamiltonian or unitary operator  $U$  with the total particle number operator  $S = \sum_i a_i^\dagger a_i$ , where  $a_i^\dagger$  and  $a_i$  represent the creation and annihilation operators, respectively. In this case, the eigenspaces of  $S$  correspond to states with fixed particle numbers, and the symmetry can be utilized to detect errors that break particle number conservation.

When the fermion system is transformed into a qubit system using the Jordan–Wigner transformation, the particle number operator can be expressed as  $S = \sum_i Z_i$ . The operator  $S$  has  $n+1$  eigenspaces with projectors defined as  $\Pi_i = \sum_{|\mathbf{x}|=i} |\mathbf{x}\rangle\langle\mathbf{x}|$ . Here,  $\mathbf{x} \in \{0, 1\}^n$  represents a bit string of length  $n$  and  $|\mathbf{x}|$  represents the number of 1 in the bit string  $\mathbf{x}$ . In this case, the operator  $V_S$  defined in Eq. (6) can be represented as

$$V_S = \sum_{\mathbf{x} \in \{0,1\}^n} \exp\left[\frac{2\pi i}{2^m} |\mathbf{x}| \right] |\mathbf{x}\rangle\langle\mathbf{x}| = R\left(\frac{2\pi}{2^m}\right)^{\otimes n}, \quad (18)$$

where  $R(\theta) = |0\rangle\langle 0| + e^{i\theta} |1\rangle\langle 1|$ . Therefore, implementing SCV for particle number conservation symmetry requires  $m = \lceil \log_2(n+1) \rceil$  qubit ancilla,  $2n \lceil \log_2(n+1) \rceil$  controlled- $R(\theta)$  gates, and quantum Fourier transform. Although noise in these operations may degrade the performance of SCV, it is effective when the target unitary  $U$  is composed of more quantum gates and contains more noise. Moreover, for large system size  $n$ , the number of ancilla scales as  $O(\log n)$ , so the effect of errors on the ancilla is expected to be much smaller than the system qubits.

To evaluate the effectiveness of SCV for particle number conservation symmetry, we consider a time evolution circuit for the  $\text{H}_2$  molecule with a Haar-random input state. Since the input state is not an eigenstate of  $S = \sum_i Z_i$ , symmetry verification cannot be applied, but SCV can be used to purify the circuit. In Fig. 5, we present the trace distance between the ideal noiseless state and the error-detected state for varying evolution time  $\theta$ . Here, we assume that the noisy circuit we implement is  $\mathcal{N} \circ \mathcal{U}$ , where  $\mathcal{U}(\cdot) = e^{i\theta H} \cdot e^{-i\theta H}$  represents the time evolution for the  $\text{H}_2$  molecule (STO-3G basis set) with  $n = 4$  and an atomic distance of 1.1 Å, and  $\mathcal{N}$  is a global depolarizing noise with error rate  $n\theta p_{\text{err}}$ . We further assume that the controlled- $R(\theta)$  gate to perform SCV is affected by a local depolarizing noise with error rate  $p_{\text{err}}$ , and set  $p_{\text{err}} = 10^{-4}$ .

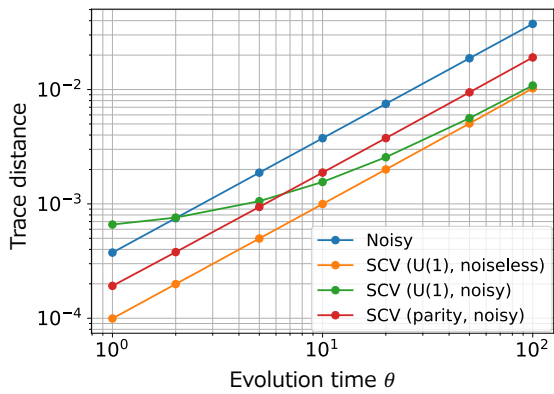


FIG. 5. Performance of SCV in detecting errors on a Hamiltonian simulation circuit for the  $H_2$  molecule. The “Noisy” line represents the trace distance between the noisy quantum state and the ideal quantum state. The “SCV (U(1), noiseless)” and “SCV (U(1), noisy)” lines represent the trace distance for the quantum state with the noise detected by SCV for the particle number operator  $\sum_i Z_i$ , where “noiseless” and “noisy” represent the results using noiseless and noisy SCV gadgets. The “SCV (parity, noisy)” line represents the result using SCV for the parity operator  $\prod_i Z_i$ , where we assume that the controlled-Pauli gates comprising the SCV gadget are affected by noise.

From Fig. 5, we observe that SCV can reduce the effect of errors when there is no noise in the SCV gadget. Meanwhile, when the SCV gadget is affected by noise, applying SCV can degrade the performance. Nevertheless, as the evolution time  $\theta$  increases and the circuit accumulates more noise, errors in the target unitary  $\mathcal{U}$  become the dominant error source, and the impact of errors on the SCV gadget diminishes. This demonstrates that when the target unitary contains a sufficient number of quantum gates relative to the SCV gadget, SCV can effectively detect noise.

Furthermore, when  $U$  commutes with the particle number operator  $\sum_i Z_i$ , it also commutes with the parity operator  $\prod_i Z_i$ . Therefore, we can apply SCV to the Pauli operator  $\prod_i Z_i$  to detect errors, whose corresponding gadget is significantly easier to implement than that for  $\sum_i Z_i$ . In Fig. 5, we also show the performance of SCV for the parity operator  $\prod_i Z_i$ , where the controlled-Pauli gates comprising the SCV gadget are affected by local depolarizing noise with an error rate  $p_{err}/100$ . Note that the difference in error rates arises because approximately 100 Clifford+T gates are required to synthesize Pauli rotation gates with high accuracy [45]. Since the SCV gadget consists of simple Clifford gates that do not require gate synthesis, SCV for the parity operator  $\prod_i Z_i$  can outperform SCV for the particle number operator  $S = \sum_i Z_i$  for small  $\theta$ . Nevertheless, when  $\theta$  increases and the noise on the target unitary becomes dominant, SCV for the particle number operator  $\sum_i Z_i$  can detect twice as much noise as SCV for the parity operator  $\prod_i Z_i$ .

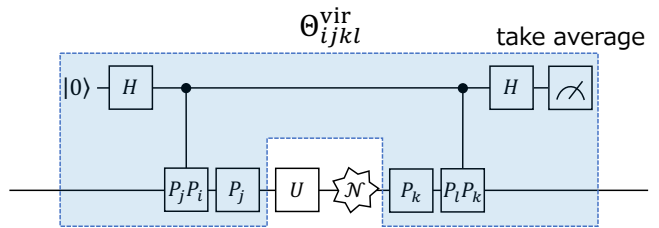


FIG. 6. A gadget to implement virtual symmetric channel verification (virtual SCV). We prepare a single-qubit ancilla initialized in  $|0\rangle$ , apply a Hadamard gate to the ancilla, apply controlled- $P_j P_i$  gate, apply  $P_j$ , the noisy channel  $\mathcal{U}_{\mathcal{N}} = \mathcal{U} \circ \mathcal{N}$ , and  $P_k$  to system qubits, apply controlled- $P_l P_k$  gate, apply a Hadamard gate to the ancilla, and measure the ancilla with the Pauli Z operator. The average of the measurement results on the ancilla qubit is taken. This operation transforms the noisy channel  $\mathcal{U}_{\mathcal{N}}(\cdot)$  into  $(\Theta_{ijkl}^{\text{vir}}(\mathcal{U}_{\mathcal{N}}))(\cdot) = \frac{1}{2}(P_k \mathcal{U}_{\mathcal{N}}(P_i \cdot P_j) P_l + P_l \mathcal{U}_{\mathcal{N}}(P_j \cdot P_i) P_k)$ .

## IV. VIRTUAL SYMMETRIC CHANNEL VERIFICATION

### A. General framework

While SCV is effective for detecting symmetry-breaking noise in noisy channels, it requires sophisticated quantum operations such as controlled- $V_S$  and quantum Fourier transform. In the near-term and early fault-tolerant regimes, implementing these operations may introduce prohibitive noise into the quantum circuits and degrade the performance of SCV. Thus, a simpler and more hardware-friendly noise-reduction technique is necessary for practical implementation.

To reduce the hardware overhead for noise purification, we introduce a virtual supermap  $\Theta_{ijkl}^{\text{vir}}$  depicted in Fig. 6. This supermap consists of a single qubit ancilla and two controlled Pauli gates, making it significantly easier to implement compared to the original SCV gadget. When we take the average of the measurement results from the ancilla qubit,  $\Theta_{ijkl}^{\text{vir}}$  maps the noisy channel  $\mathcal{U}_{\mathcal{N}}$  to a virtual map represented as

$$(\Theta_{ijkl}^{\text{vir}}(\mathcal{U}_{\mathcal{N}}))(\cdot) = \frac{1}{2}(P_k \mathcal{U}_{\mathcal{N}}(P_i \cdot P_j) P_l + P_l \mathcal{U}_{\mathcal{N}}(P_j \cdot P_i) P_k). \quad (19)$$

It should be noted that  $\Theta_{ijkl}^{\text{vir}}(\mathcal{U}_{\mathcal{N}})$  is a virtual map, which can only be used for the task of expectation value estimation.

Using the virtual supermap  $\Theta_{ijkl}^{\text{vir}}$ , SCV can be virtually implemented with much lower hardware overhead. For simplicity, suppose we aim to estimate the expectation value of an observable  $O$  for a quantum state  $\mathcal{U}(\rho)$  using SCV. In this case, the error-detected expectation value is given by

$$\frac{\text{tr}[(\Theta_S^{\text{det}}(\mathcal{U}_{\mathcal{N}}))(\rho)O]}{\text{tr}[(\Theta_S^{\text{det}}(\mathcal{U}_{\mathcal{N}}))(\rho)]}. \quad (20)$$



The key idea to reduce the hardware overhead in calculating Eq. (20) is to decompose the projector  $\Pi_i$  using Pauli operators as  $\Pi_i = \sum_j \pi_{ij} P_j$ . By similarly decomposing the supermap  $\Theta_S^{\text{det}}$ , we have

$$\Theta_S^{\text{det}} = \sum_{ijkl} \alpha_{ijkl} \Theta_{ijkl}^{\text{vir}} = \gamma \sum_{ijkl} \frac{|\alpha_{ijkl}|}{\gamma} \text{sgn}(\alpha_{ijkl}) \Theta_{ijkl}^{\text{vir}}, \quad (21)$$

where  $\alpha_{ijkl} = \sum_{ab} \pi_{ai} \pi_{bj} \pi_{ak} \pi_{bl}$ ,  $\gamma = \sum_{ijkl} |\alpha_{ijkl}|$ , and  $\text{sgn}(\alpha_{ijkl})$  represents the sign of  $\alpha_{ijkl}$ . Thus, Eq. (20) can also be decomposed as

$$\frac{\sum_{ijkl} \frac{|\alpha_{ijkl}|}{\gamma} \text{sgn}(\alpha_{ijkl}) \text{tr}[(\Theta_{ijkl}^{\text{vir}}(\mathcal{U}_N))(\rho)O]}{\sum_{ijkl} \frac{|\alpha_{ijkl}|}{\gamma} \text{sgn}(\alpha_{ijkl}) \text{tr}[(\Theta_{ijkl}^{\text{vir}}(\mathcal{U}_N))(\rho)]}. \quad (22)$$

This value can be obtained using the circuit in Fig. 6 with the following protocol:

1. For  $s = 1, \dots, N$ , repeat the following steps:
  - (a) Sample  $i, j, k, l$  with probability  $|\alpha_{ijkl}|/\gamma$ .
  - (b) Run the circuit illustrated in Fig. 6 and measure the system with the observable  $O$ .
  - (c) Record the  $Z$  measurement of the ancilla as  $a_s$  and the product of  $a_s$  and the  $O$  measurement as  $b_s$ .
  - (d) Replace  $a_s$  and  $b_s$  with  $\text{sgn}(\alpha_{ijkl})a_s$  and  $\text{sgn}(\alpha_{ijkl})b_s$ .
2. Calculate  $a = \frac{1}{N} \sum_s a_s$  and  $b = \frac{1}{N} \sum_s b_s$ .
3. Output  $b/a$ .

We refer to this simplified SCV protocol for expectation value estimation as *virtual symmetric channel verification* (virtual SCV).

Virtual SCV generalizes virtual symmetry verification methods [26–29] to the channel level. Indeed, virtual SCV can be implemented even when the input state  $\rho$  lacks the same symmetry as the unitary  $U$ . Moreover, while our discussion focused on implementing virtual SCV just before measurement, virtual SCV can also be applied to parts of the quantum circuit. Thus, similar to SCV, virtual SCV can be implemented when different quantum operations in the circuit exhibit different symmetric structures.

Compared to SCV, virtual SCV offers significantly lower hardware overhead. While SCV requires  $\lceil \log_2 M \rceil$  qubits for the ancilla, virtual SCV requires only a single-qubit ancilla. Moreover, SCV involves sophisticated quantum operations such as controlled- $V_S$  and quantum Fourier transform, whereas virtual SCV replaces these with controlled-Pauli operations, which are Clifford operations. In the early fault-tolerant regime, Clifford gates are expected to be easier to implement than non-Clifford gates, as they do not require gate synthesis using Clifford+T gates [45, 50, 51]. Thus, virtual SCV is much

easier to implement than SCV, relying only on Clifford gates.

Another advantage of virtual SCV is its robustness to noise in the ancilla qubit. For example, let us assume that depolarizing noise with error probability  $p$  affects the ancilla qubit at any point during computation. While such noise may propagate to the system qubits, its effect is removed when averaging the measurement results. Under the depolarizing noise on the ancilla, the virtual channel  $\Theta_{ijkl}^{\text{vir}}(\mathcal{U}_N)$  is affected as

$$\left(1 - \frac{4}{3}p\right) \frac{1}{2} (P_k \mathcal{U}_N(P_i \cdot P_j) P_l + P_i \mathcal{U}_N(P_j \cdot P_i) P_k), \quad (23)$$

indicating that the noise on the ancilla adds only a constant factor of  $1 - \frac{4}{3}p$  to the original channel. Since this constant factor is removed during state normalization in Eq. (22), the effect of ancilla noise is completely removed. Furthermore, idling errors on the ancilla qubit during execution of the noisy channel  $\mathcal{U}_N$  can be twirled with single-qubit Clifford unitaries into depolarizing noise [52, 53]. Thus, the effect of arbitrary noise beyond depolarizing noise can be removed.

Despite these advantages, virtual SCV has certain drawbacks. The first is that virtual SCV is a virtual protocol and can only be used for expectation value estimation. However, since expectation value estimation can be used as a subroutine for various tasks such as phase estimation [36, 54], virtual SCV remains applicable to many early fault-tolerant algorithms. Another drawback is its sampling overhead. The leading factor of the sampling overhead for virtual protocols is the square of the inverse of the denominator in Eq. (22) [27]. This overhead scales as  $\gamma^2 \text{tr}[(\Theta_S^{\text{det}}(\mathcal{U}_N))(\rho)]^{-2} \sim \gamma^2 (1+p)^2$  when symmetry-breaking errors occur with probability  $p$ . For  $L$  noisy channels  $\mathcal{U}_N$ , applying virtual SCV to each channel results in sampling overhead scaling as  $O((1+p)^{2L})$ , which is quadratically larger than SCV. Moreover, when applying virtual SCV for the particle number operator  $S = \sum_i Z_i$ ,  $\gamma$  grows exponentially with the number of system qubits  $n$  and becomes intractable. Nevertheless, for many practical use cases stated below,  $\gamma$  is equal to 1, so it does not contribute to an increase in the sampling overhead.

## B. Application to Pauli symmetry

As discussed in Sec. III B, the SCV gadget for a single Pauli operator  $Q$  requires only a single-qubit ancilla and two controlled- $Q$  gates, whose hardware overhead is comparable with virtual SCV. Therefore, when implementing SCV for a single Pauli operator, there is no advantage in employing virtual SCV (except the fact that virtual SCV is robust against the noise in the ancilla). However, the SCV gadget designed for a set of commuting Pauli operators  $Q_U^{\text{com}}$ , which concatenates multiple SCV gadgets for different Pauli operators, requires  $r$  ancilla qubits and  $2r$

controlled-Pauli gates as depicted in Fig. 3. In this case, virtual SCV can significantly reduce hardware overhead.

The SCV gadget  $\Theta_{\mathcal{Q}_U^{\text{com}}}^{\text{det}}$  maps the noisy channel  $\mathcal{U}_{\mathcal{N}}$  to

$$\begin{aligned} & \sum_{i_1 j_1 \dots i_r j_r} \Pi_{i_1 \dots i_r} \mathcal{U}_{\mathcal{N}}(\Pi_{i_1 \dots i_r}^\dagger \cdot \Pi_{i_1 \dots i_r}) \Pi_{i_1 \dots i_r}^\dagger \\ &= \frac{1}{|\mathcal{Q}_U^{\text{com}}|^2} \sum_{Q_i, Q_j \in \mathcal{Q}_U^{\text{com}}} Q_i \mathcal{U}_{\mathcal{N}}(Q_i \cdot Q_j) Q_j, \end{aligned} \quad (24)$$

where  $\Pi_{i_1 \dots i_r} = \Pi_{i_1}^1 \dots \Pi_{i_r}^r$  with  $\Pi_{i_k}^k = \frac{1}{2}(I + (-1)^{i_k} Q_k)$  being the projector onto the eigenspace of  $Q_k$  corresponding to the eigenvalue  $(-1)^{i_k}$ . This means that the SCV gadget  $\Theta_{\mathcal{Q}_U^{\text{com}}}^{\text{det}}$  can be represented as

$$\Theta_{\mathcal{Q}_U^{\text{com}}}^{\text{det}} = \frac{1}{|\mathcal{Q}_U^{\text{com}}|^2} \sum_{Q_i, Q_j \in \mathcal{Q}_U^{\text{com}}} \Theta_{ijij}^{\text{vir}}, \quad (25)$$

where  $\Theta_{ijij}^{\text{vir}}$  is the virtual supermap depicted in Fig. 6 with  $P_i = Q_i, P_j = Q_j, P_k = Q_i, P_l = Q_j$ . Therefore, we have  $\gamma = 1$ , and virtual SCV can be implemented by randomly and uniformly sampling  $Q_i, Q_j \in \mathcal{Q}_U^{\text{com}}$ . This approach reduces the number of ancilla qubits from  $r$  to 1 and the number of controlled-Pauli gates from  $2r$  to 2, and the ancilla becomes robust against its noise.

### C. Mitigating Errors on Idling Qubits with Virtual Symmetric Channel Purification

One of the powerful applications of virtual SCV is the mitigation of errors on idling qubits. Let us consider the case where the ideal channel is the identity channel  $\mathcal{I}$  for a single qubit ( $n = 1$ ), which is affected by an idling error  $\mathcal{N}^{\circ L}$ , where  $\mathcal{N}$  represents the noise per time step and  $L$  represents the idle time. Since arbitrary error anti-commutes with at least one element of  $\mathcal{Q}_I^{\text{com}} = \{I, X, Y, Z\}$ , we can apply the SCV gadget  $\Theta_{\mathcal{Q}_I^{\text{com}}}^{\text{det}}$  to completely detect the idling error  $\mathcal{N}^{\circ L}$ . However, as depicted in Fig. 7 (a), the ancilla qubit used in the SCV gadget  $\Theta_{\mathcal{Q}_I^{\text{com}}}^{\text{det}}$  is also affected by the same idling error  $\mathcal{N}^{\circ L}$ , which degrades the performance of SCV.

To overcome this limitation, we employ virtual SCV to mitigate the idling error  $\mathcal{N}^{\circ L}$ . While the same noise  $\mathcal{N}$  affects the ancilla qubit, virtual SCV is robust against depolarizing noise in the ancilla. Therefore, when we assume that  $\mathcal{N}$  is depolarizing noise, almost all the noise in the virtual SCV gadget does not impact the error-mitigation performance (see Fig. 7 (b)). The only remaining error is the one on the system qubit after the controlled Pauli gate. Figure 7 (c) illustrates the performance difference in (virtually) detecting errors between SCV and virtual SCV. We observe that while the error reduction is limited in SCV, virtual SCV significantly reduces the impact of idling errors.

As a practical application of virtual SCV in mitigating idling errors, we consider its use in suppressing errors in idling system qubits during SELECT operations.

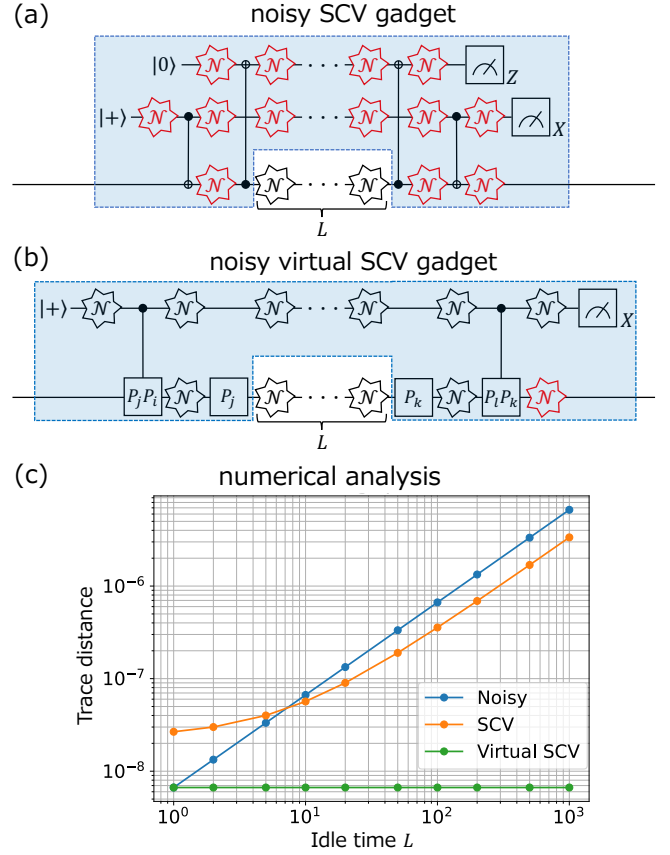


FIG. 7. Schematic illustration of (virtually) detecting idling errors  $\mathcal{N}^{\circ L}$  using (a) a noisy SCV gadget and (b) a noisy virtual SCV gadget. The noise channel depicted in red degrades the performance of (virtual) error detection, while the noise channel depicted in black does not affect performance. Here, we assume that the noise channel  $\mathcal{N}$  is depolarizing noise. Panel (c) shows the trace distance between the noiseless and noisy quantum states affected by the idling error  $\mathcal{N}^{\circ L}$ , where the noisy SCV and virtual SCV gadgets in panels (a) and (b) are used to suppress the effect of noise. The error rate of the depolarizing noise is set to  $p_{\text{err}} = 10^{-8}$ .

SELECT operations are widely used in various quantum algorithms, such as phase estimation and Hamiltonian simulation based on qubitization [30–33]. In SELECT operations, quantum gates are applied sparsely to system qubits, leading to long idle times. Thus, virtual SCV can be employed to mitigate such idling errors in system qubits.

As a demonstration, we consider the SELECT operation of the 2D Fermi-Hubbard model on a square lattice with linear system size of  $M$  and system qubit count  $n = 2M^2$ , as discussed in Ref. [31]. We provide the Hamiltonian and the circuit structure of the corresponding SELECT operation in Appendix B. We assume that all quantum gates and idling qubits are subject to local depolarizing noise with an error rate of  $p_{\text{err}} = 10^{-8}$ , and calculate the total error rate of the SELECT opera-

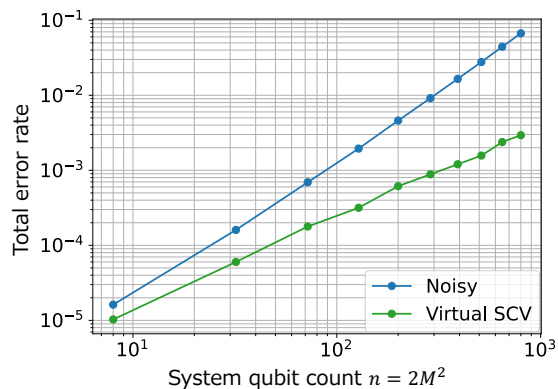


FIG. 8. The total error rate of the SELECT operation of the 2D Fermi-Hubbard model on a square lattice with linear system size of  $M$  and system qubit count  $n = 2M^2$ , proposed in Ref. [31]. The “Noisy” and “Virtual SCV” lines represent the results without and with virtual SCV, respectively. We assume that all quantum gates and idling qubits are subject to local depolarizing noise with an error rate of  $p_{\text{err}} = 10^{-8}$ .

tion with and without virtual SCV in Fig. 8. Without virtual SCV, SELECT operation has  $O(n)$  depth, so each system qubit experiences  $O(n)$  idling errors, and the total error rate scales as  $O(n^2)$ . In contrast, when virtual SCV is applied, these errors are mitigated, and only  $O(1)$  errors per system qubit remain. Consequently, the dominant error source becomes the  $O(n \log n)$  errors on the  $O(\log n)$  ancilla qubits required for qubitization. Therefore, as illustrated in Fig. 8, applying virtual SCV to idling system qubits enables a quadratic reduction in the total error rate. Notably, this reduction is not limited to this specific model but can be generalized to arbitrary Fermi-Hubbard models with short-range 2-body interactions under the Jordan–Wigner transformation, as well as lattice spin models with short-range 2-body interactions. In these cases, if the depth of the SELECT is  $d$ , then the total error rate can be mitigated from  $O(nd)$  to  $O(\log(n)d)$ . Additionally, the same ancilla qubit can be used to perform virtual SCV on all  $n$  system qubits. Thus, only a single additional ancilla qubit is required to implement virtual SCV, regardless of the number of system qubits  $n$ .

## V. CORRECTING ERRORS USING SYMMETRIC CHANNEL VERIFICATION

### A. General framework

Since SCV post-selects the measurement results on the ancilla qubit, it probabilistically provides a purified channel, resulting in an additional sampling overhead of  $O((1+p)^L)$  to detect the effect of noise. Furthermore, virtual SCV requires a quadratically larger sampling overhead of  $O((1+p)^{2L})$  for its implementation. While these

methods are effective when the total error rate  $pL$  is small, they become inefficient for larger error rates due to the exponential growth in the sampling overhead.

To reduce the sampling overhead, feedback controls can be applied to the system qubits based on the measurement results from the ancilla qubits, instead of post-selecting them. This approach allows *correction* of symmetry-breaking errors on noisy channels without introducing additional sampling overhead. As discussed in Sec. II, feedback controls can be implemented using a superchannel  $\Theta^{\text{cor}}$  defined in Eq. (3) by adding controlled operation corresponding to the feedback control into the unitary channel  $\mathcal{U}_D$ . Thus, applying feedback control to the SCV gadget  $\Theta_S^{\text{det}}$  in Fig. 2 is equivalent to inserting an additional unitary operator before the measurement and discarding the measurement results. The performance of such deterministic channel purification protocols is summarized in the following theorem:

**Theorem 2.** *Let  $\Theta_S^{\text{cor}}$  denote a quantum superchannel where an additional unitary operator is inserted before the measurement in the circuit depicted in Fig. 2, and the measurement results are discarded. Then,  $\Theta_S^{\text{cor}}$  can correct the noise  $\mathcal{N}(\cdot) = \sum_{j=0}^K N_j \cdot N_j^\dagger$  on the noisy channel  $\mathcal{U}_N$ , i.e.,  $\Theta_S^{\text{cor}}(\mathcal{U}_N) = \mathcal{U}$ , if and only if for all  $j, k \in \{0, \dots, K\}$*

$$\sum_i \Pi_i N_j^\dagger N_k \Pi_i \propto I_n. \quad (26)$$

Theorem 2 can be derived by interpreting the initial half of the SCV gadget  $\Theta_S^{\text{det}}$  as an encoding process on a quantum error-correcting code. By applying the quantum error correction condition [55, 56], we arrive at Theorem 2. For a detailed proof, we refer the reader to Appendix A.

### B. Application to Pauli symmetry

As an application of SCV for error correction, consider a quantum channel under Pauli symmetry. Following the setup in Sec. III B, we analyze the case where the noise channel  $\mathcal{N}(\cdot) = \sum_{i=0}^K P_i \cdot P_i$  is Pauli noise as represented in Eq. (11). By applying feedback controls based on the measurement results from the SCV gadget for  $\mathcal{Q}_U^{\text{com}}$  in Fig. 3, Pauli errors can be corrected to some extent. The performance of such deterministic channel purification protocols under Pauli symmetry is characterized by the following theorem:

**Corollary 2.** *Let  $\Theta_{\mathcal{Q}_U^{\text{com}}}^{\text{cor}}$  denote a quantum superchannel where feedback controls using Pauli operators are applied according to the measurement results from the SCV gadget for  $\mathcal{Q}_U^{\text{com}}$  in Fig. 3. Then,  $\Theta_{\mathcal{Q}_U^{\text{com}}}^{\text{cor}}$  can correct the Pauli noise Eq. (11) on the noisy channel  $\mathcal{U}_N$ , i.e.,  $\Theta_{\mathcal{Q}_U^{\text{com}}}^{\text{cor}}(\mathcal{U}_N) = \mathcal{U}$ , if and only if*

$$\mathcal{P}_N^{\text{cor}} \cap \mathcal{Q}_U = \emptyset, \quad (27)$$

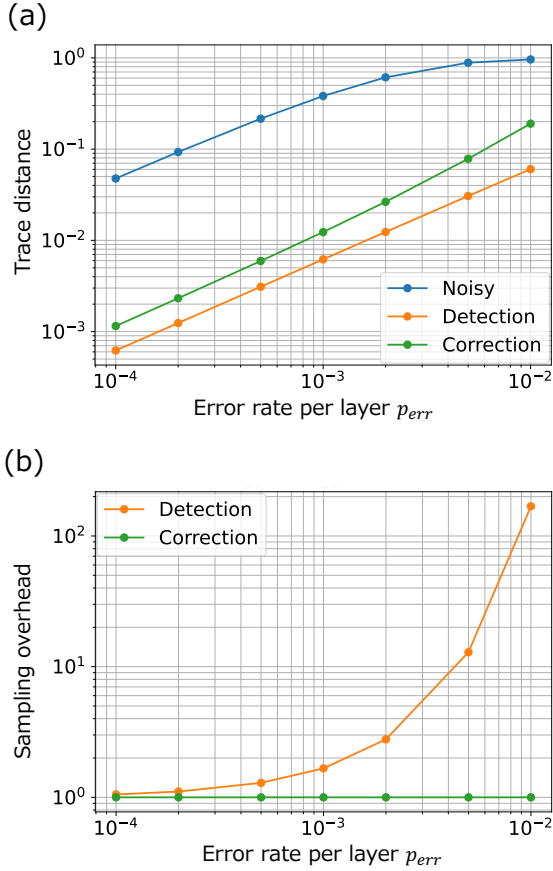


FIG. 9. Performance of SCV in detecting and correcting errors in Hamiltonian simulation circuits  $U = e^{-i\theta H}$ , where the Hamiltonian is given by  $H = -\sum_{S \in \mathcal{S}} S$  and  $\mathcal{S}$  is the set of stabilizers of the  $[[5, 1, 3]]$  code. Panel (a) shows the trace distance between the ideal quantum state and the noisy quantum state, purified by the error detection gadget  $\Theta_{\mathcal{Q}_U}^{\text{det}}$  or the error correction gadget  $\Theta_{\mathcal{Q}_U}^{\text{cor}}$ . Panel (b) shows the sampling overhead required for purification.

where  $\mathcal{P}_N^{\text{cor}} = \{\pm 1, \pm i\} \cdot \{P_i P_j\}_{i,j=0}^K \setminus \{I_n\}$  and  $\mathcal{Q}_U$  is defined in Eq. (13).

Corollary 2 implies that if  $\mathcal{Q}_U$  consists of Pauli operators with weights greater than or equal to  $d$ , arbitrary  $(d-1)/2$ -qubit errors can be corrected. Meanwhile, when focusing on detecting errors, Corollary 1 indicates that arbitrary  $(d-1)$ -qubit errors can be detected. This result is consistent with state-level error correction and detection protocols. An interesting example is the time evolution circuit of the lattice fermion model using the Majorana loop stabilizer code [57]. In this case, we have  $d = 3$ , meaning that arbitrary single-qubit errors can be corrected. Another example is the time evolution  $U = e^{i\theta H}$  of the Hamiltonian  $H = -\sum_{S \in \mathcal{S}} a_S S$ , where  $\mathcal{S}$  is the set of stabilizers of a stabilizer code with distance  $d$  and  $a_S \in \mathbb{R}$  is a coefficient for the stabilizer  $S$ . In this case, when the input state to the unitary is within the code space, the usual state-level error correction can

be applied to correct errors. However, if the input state spans multiple eigenspaces, syndrome measurement may destroy the state, so the usual state-level error correction cannot be applied. Even in this case, assuming that the SCV gadget  $\Theta_{\mathcal{Q}_U}^{\text{cor}}$  can be applied without additional errors, arbitrary  $(d-1)/2$ -qubit errors can be corrected using the SCV gadget  $\Theta_{\mathcal{Q}_U}^{\text{cor}}$ .

To evaluate the performance of SCV in correcting errors under noise in the SCV gadget  $\Theta_{\mathcal{Q}_U}^{\text{cor}}$ , we consider the time evolution  $U = e^{-i\theta H}$  of the Hamiltonian  $H = -\sum_{S \in \mathcal{S}} S$ , where  $\mathcal{S}$  is the set of stabilizers of the  $[[5, 1, 3]]$  code. We model the noisy circuit as  $\bigcirc_{l=1}^L \mathcal{N}_l \circ \mathcal{U}_l$ , where  $\mathcal{N}_l$  represents local depolarizing noise with an error rate  $p_{\text{err}}$ , and  $\mathcal{U}_l(\cdot) = e^{i(\theta/L)H} \cdot e^{-i(\theta/L)H}$  corresponds to a single time step. Furthermore, we assume that the controlled Pauli gates composing the SCV gadgets are also affected by local depolarizing noise with an error rate of  $p_{\text{err}}/100$ . This difference in error rates arises because approximately 100 Clifford+T gates are required to synthesize Pauli rotation gates with an accuracy of  $10^{-6}$  [45]. We set  $\theta = 2\pi$  and  $L = 100$ , and use a Haar-random state as the input state.

Our results are shown in Fig. 9. When noise is present in the SCV gadgets, performing error detection or correction leads to a constant reduction in the error rate. This is because, although the SCV gadgets can detect or correct arbitrary single-qubit errors on system qubits, the noise in the SCV gadgets dominates overall performance. While we expect that the effect of such noise can be removed by extending fault-tolerant error correction protocols to the channel level, we leave this analysis as future work. Comparing the performance of the error detection gadget  $\Theta_{\mathcal{Q}_U}^{\text{det}}$  and the error correction gadget  $\Theta_{\mathcal{Q}_U}^{\text{cor}}$ , we observe that the error detection gadget achieves higher accuracy. However, it incurs significant sampling overhead, whereas the error correction gadget  $\Theta_{\mathcal{Q}_U}^{\text{cor}}$  can correct errors without additional sampling overhead.

## VI. LIMITATIONS OF CHANNEL PURIFICATION USING CLIFFORD UNITARIES

In previous sections, we did not explicitly impose restrictions on the operations used for the task of channel purification. From a practical viewpoint in the early fault-tolerant regime, one of the most important restrictions is to use only Clifford gates so that the impact of errors within the purification gadget is minimized. This is because Clifford gates are expected to be easier to implement, especially compared to arbitrary angle Pauli rotations which require gate synthesis [45, 50, 51].

In this section, we investigate the fundamental limitations of purifying noisy quantum channels using only Clifford unitaries for the purification gadget. In particular, we focus on the purification of a Hamiltonian simulation unitary, given by  $\mathcal{U}(\cdot) = e^{i\theta H} \cdot e^{-i\theta H}$ , when it is subject to Pauli noise  $\mathcal{N} = \sum_{i=0}^K p_i P_i \cdot P_i$  as defined in Eq. (11). We

derive the necessary and sufficient conditions for the noise to be completely *detectable* and *correctable* using Clifford unitaries, formally presented as Theorem 3 and 4, respectively. We further demonstrate that these conditions coincide with those required for the noise to be both completely detectable and correctable using SCV under Pauli symmetry. When such conditions are not satisfied, the SCV cannot eliminate the entire effect of noise. Nonetheless, as presented as in Theorem 5, we can derive an upper bound on the fidelity of the purified channel, and also show that this bound is saturated by SCV under Pauli symmetry. These results demonstrate that SCV under Pauli symmetry provides the best channel purification protocol under the constraint of Clifford unitaries.

We first consider the fundamental limitations in detecting errors in the noisy channel  $\mathcal{U}_{\mathcal{N}} = \mathcal{N} \circ \mathcal{U}$ , when only Clifford gates are used for the entangling operations between the system and ancilla. As discussed in Sec. II, detecting errors corresponds to applying a supermap  $\Theta^{\text{det}}$ , defined in Eq. (1). It is convenient to recall that  $\Theta^{\text{det}}$  transforms the noisy channel  $\mathcal{U}_{\mathcal{N}}$  into a trace non-increasing map  $\Theta^{\text{det}}(\mathcal{U}_{\mathcal{N}})$  whose action is given as

$$\rho \mapsto \langle 0^m | \mathcal{U}_{\text{D}} \circ (\mathcal{U}_{\mathcal{N}} \otimes \mathcal{I}_a) \circ \mathcal{U}_{\text{E}}(\rho \otimes |0^m\rangle\langle 0^m|) | 0^m \rangle. \quad (28)$$

When we are restricted to using only Clifford gates for error detection, the unitaries  $\mathcal{U}_{\text{E}}(\cdot) = U_{\text{E}} \cdot U_{\text{E}}^\dagger$  and  $\mathcal{U}_{\text{D}}(\cdot) = U_{\text{D}} \cdot U_{\text{D}}^\dagger$ , which construct the supermap  $\Theta^{\text{det}}$ , are constrained to  $(n+m)$ -qubit Clifford unitaries. Let us denote such a supermap consisting of Clifford unitaries as  $\Theta_{\text{Clif}}^{\text{det}}$ . For the error detection supermap  $\Theta_{\text{Clif}}^{\text{det}}$ , we can identify the detectable noise via the following theorem.

**Theorem 3.** *Let  $\mathcal{U}(\cdot) = e^{i\theta H} \cdot e^{-i\theta H}$  be an  $n$ -qubit unitary channel and  $\mathcal{N}(\cdot) = \sum_{i=0}^K p_i P_i \cdot P_i$  be a Pauli noise defined in Eq. (11). Then, there exists an error detection supermap  $\Theta_{\text{Clif}}^{\text{det}}$  that can detect the set of errors  $\mathcal{P}_{\mathcal{N}}^{\text{det}} = \{P_i\}_{i=1}^K$  as*

$$\forall \theta, \Theta_{\text{Clif}}^{\text{det}}(\mathcal{N}_{P_i} \circ \mathcal{U}) = \delta_{i0} \mathcal{U}, \quad (29)$$

if and only if

$$\mathcal{P}_{\mathcal{N}}^{\text{det}} \cap \mathcal{Q}_H = \emptyset. \quad (30)$$

Here,  $\mathcal{N}_{P_i}(\cdot) = P_i \cdot P_i$ ,  $\delta_{ij}$  represents the Kronecker delta, and  $\mathcal{Q}_H$  is a set of Pauli operators generated from Pauli operators with non-zero coefficients in the Pauli expansion of  $H$ , as defined in Eq. (13).

The key idea for proving the necessary condition of Theorem 3 is to interpret the application of the Clifford unitary  $U_{\text{E}}$  as encoding into a stabilizer code with a code space spanned by  $U_{\text{E}}|\psi\rangle|0^m\rangle$ . Under Eq. (29), we can show that all elements except  $I^{\otimes n+m}$  in  $\mathcal{Q}_H \otimes \{I\}^{\otimes m}$  are non-trivial logical Pauli operators. Since detectable errors cannot be non-trivial logical Pauli operators, we obtain Eq. (30). To show sufficiency, we consider detecting noise with SCV under Pauli symmetry, which we

have discussed in Sec. III B. Interestingly, the necessary condition in Eq. (30) exactly matches the condition for detectable noise using SCV under Pauli symmetry, which is characterized in Corollary 1. This implies that when error detection for the noisy channel is restricted to Clifford operations, we cannot detect more noise than using SCV under Pauli symmetry. Therefore, it suffices to use SCV under the restriction, demonstrating the optimality of our protocol. See Appendix A for the full proof.

Let us comment on the necessary and sufficient condition in Eq. (30). This condition implies that Pauli errors included in the Hamiltonian cannot be detected; such errors are indistinguishable from the unitary  $e^{i\theta H}$ . Moreover, Eq. (30) implies that, if  $\mathcal{Q}_H$  consists of Pauli operators with weights greater than or equal to  $d$ , SCV can detect arbitrary  $(d-1)$ -qubit errors. A notable example is the Heisenberg model discussed in Sec. III B. For this Hamiltonian,  $\mathcal{Q}_H$  consists of weight-2 or higher Pauli operators, allowing the detection of arbitrary single-qubit errors.

Next, we consider the limitations in correcting errors in the noisy channel  $\mathcal{U}_{\mathcal{N}}$  using Clifford gates. As discussed in Sec. II, correcting errors corresponds to applying a superchannel  $\Theta^{\text{cor}}$ , defined in Eq. (3), which transforms the noisy channel  $\mathcal{U}_{\mathcal{N}}$  into a quantum channel  $\Theta^{\text{cor}}(\mathcal{U}_{\mathcal{N}})$ , defined as

$$\rho \mapsto \text{tr}_a[\mathcal{U}_{\text{D}} \circ (\mathcal{U}_{\mathcal{N}} \otimes \mathcal{I}_a) \circ \mathcal{U}_{\text{E}}(\rho \otimes |0^m\rangle\langle 0^m|)]. \quad (31)$$

When we are restricted to using only Clifford gates for error correction, the unitaries  $\mathcal{U}_{\text{E}}(\cdot) = U_{\text{E}} \cdot U_{\text{E}}^\dagger$  and  $\mathcal{U}_{\text{D}}(\cdot) = U_{\text{D}} \cdot U_{\text{D}}^\dagger$ , which construct the superchannel  $\Theta^{\text{cor}}$ , are constrained to  $(n+m)$ -qubit Clifford unitaries. Let us denote such a superchannel consisting of Clifford unitaries as  $\Theta_{\text{Clif}}^{\text{cor}}$ . For the error correction superchannel  $\Theta_{\text{Clif}}^{\text{cor}}$ , the correctable noise can be characterized via the following theorem.

**Theorem 4.** *Let  $\mathcal{U}(\cdot) = e^{i\theta H} \cdot e^{-i\theta H}$  be an  $n$ -qubit unitary channel and  $\mathcal{N}(\cdot) = \sum_{i=0}^K p_i P_i \cdot P_i$  be a Pauli noise defined in Eq. (11). Then, there exists an error correction superchannel  $\Theta_{\text{Clif}}^{\text{cor}}$  that satisfies*

$$\forall \theta, \Theta_{\text{Clif}}^{\text{cor}}(\mathcal{U}_{\mathcal{N}}) = \mathcal{U}, \quad (32)$$

if and only if

$$\mathcal{P}_{\mathcal{N}}^{\text{cor}} \cap \mathcal{Q}_H = \emptyset. \quad (33)$$

Here,  $\mathcal{P}_{\mathcal{N}}^{\text{cor}} = \{\pm 1, \pm i\} \cdot \{P_i P_j\}_{i,j=0}^K \setminus \{I_n\}$ ,  $\mathcal{U}_{\mathcal{N}} = \mathcal{N} \circ \mathcal{U}$ , and  $\mathcal{Q}_H$  is a set of Pauli operators generated from Pauli operators with non-zero coefficients in the Pauli expansion of  $H$ , as defined in Eq. (13).

The proof of Theorem 4 is essentially the same as that of Theorem 3. The only difference is that we use the quantum error correction condition instead of the quantum error detection condition [55, 56], so  $\mathcal{P}_{\mathcal{N}}^{\text{det}} = \{P_i\}_{i=1}^K$  in Eq. (30) becomes  $\mathcal{P}_{\mathcal{N}}^{\text{cor}} = \{\pm 1, \pm i\} \cdot \{P_i P_j\}_{i,j=0}^K \setminus \{I_n\}$ . See Appendix A for the full proof. The interesting aspect

of Theorem 4 is that the necessary and sufficient condition in Eq. (33) exactly matches the condition for correctable noise using SCV under Pauli symmetry, which is characterized in Corollary 2. Therefore, when we are restricted to using Clifford gates to correct errors in the noisy channel, we cannot correct more noise than using SCV under Pauli symmetry. This represents the sufficiency and optimality of applying SCV in this scenario.

We remark that our error correction condition is more strict than those required in covariant quantum error correction [58, 59]. In Refs. [58, 59], the authors aimed to purify the noisy channel  $\mathcal{U}_N$  into a noiseless channel  $\mathcal{U}'(\cdot) = e^{i\theta H'} \cdot e^{-i\theta H'}$ , where they allow the Hamiltonian to change from  $H$  to  $H' \not\propto I_n$ . Specifically, they showed that the transformation

$$\forall \theta, \Theta_{\text{Clif}}^{\text{cor}}(\mathcal{U}_N) = \mathcal{U}' \quad (34)$$

is possible if and only if

$$\mathcal{Q}'_H \not\subset \mathcal{P}_N^{\text{cor}}, \quad (35)$$

where  $\mathcal{Q}'_H$  is a set of Pauli operators with non-zero coefficients in the Pauli expansion of  $H$ , as defined in Eq. (12). Even though the Hamiltonian may change when correcting errors, this transformation is useful for estimating  $\theta$  at the Heisenberg limit [60]. The condition in Eq. (35) implies that, if there is at least one term in the Hamiltonian that is not included in the set  $\mathcal{P}_N^{\text{cor}}$ , then we can preserve that term while correcting all the errors. More precisely, Eq. (35) states that there exists a Pauli operator  $Q \in \mathcal{Q}'_H$  such that  $Q \notin \mathcal{P}_N^{\text{cor}}$ . Under this condition, we can achieve Eq. (34) by setting  $H' \propto Q$ . However, our goal in channel purification is not to preserve at least one term of the Hamiltonian, but to preserve the entire Hamiltonian  $H$  when correcting errors. Therefore, all elements in  $\mathcal{Q}'_H$  (including Pauli operators generated from them) should not be in the set  $\mathcal{P}_N^{\text{cor}}$ , resulting in the condition in Eq. (33) in Theorem 4.

Finally, we consider the case where the effect of noise cannot be entirely eliminated. In Theorem 3 and Theorem 4, we aim to recover the ideal noiseless channel  $\mathcal{U}$  itself by detecting and correcting all noise components. However, as seen in our numerical results, such channel purification is not possible in many practical setups, even when noise is absent in the SCV gadget. In such cases, we aim to construct  $\Theta^{\text{cor}}$  so that the purified channel  $\Theta^{\text{cor}}(\mathcal{U}_N)$  becomes as close as possible to the noiseless channel  $\mathcal{U}$ . To quantify the performance of such approximate purification, we define the worst-case fidelity between two quantum channels  $\mathcal{E}$  and  $\mathcal{F}$  as

$$F(\mathcal{E}, \mathcal{F}) = \min_{\rho} F(\mathcal{I} \otimes \mathcal{E}(\rho), \mathcal{I} \otimes \mathcal{F}(\rho)), \quad (36)$$

where  $F$  on the right-hand side represents the fidelity between two quantum states, and  $\mathcal{I}$  is the identity channel of the same dimension as  $\mathcal{E}$ . Our goal is to derive an upper bound on the worst-case fidelity when the superchannel  $\Theta_{\text{Clif}}^{\text{cor}}$  is implemented using Clifford unitaries.

For simplicity, let us consider the case of correcting Pauli noise affecting Pauli rotation gates. Since arbitrary Pauli rotation gates can be transformed into Pauli-Z rotation gates by conjugating them with Clifford gates, we focus specifically on purifying the Pauli-Z rotation gate  $\mathcal{U}(\cdot) = e^{-i\frac{\theta}{2}Z} \cdot e^{i\frac{\theta}{2}Z}$  under single-qubit Pauli noise  $\mathcal{N}(\cdot) = p_0 \cdot + p_x X \cdot X + p_y Y \cdot Y + p_z Z \cdot Z$ . By applying an upper bound on the worst-case fidelity obtained from the resource-theoretic analysis in Ref. [38], we establish the following theorem.

**Theorem 5.** *Let  $\mathcal{U}(\cdot) = e^{-i\frac{\theta}{2}Z} \cdot e^{i\frac{\theta}{2}Z}$  be a Pauli-Z rotation gate with  $0 \leq \theta \leq \pi/4$ , and let  $\mathcal{N}(\cdot) = p_0 \cdot + p_x X \cdot X + p_y Y \cdot Y + p_z Z \cdot Z$  be a single-qubit Pauli noise channel affecting  $\mathcal{U}$ . Then, the superchannel  $\Theta_{\text{Clif}}^{\text{cor}}$  satisfies*

$$F(\Theta_{\text{Clif}}^{\text{cor}}(\mathcal{U}_N), \mathcal{U}) \leq \frac{1 + \cos \theta}{2} \left( (p_0 + p_z) R\left(\theta, \frac{p_z}{p_0 + p_z}\right) + (p_x + p_y) R\left(\theta, \frac{p_y}{p_x + p_y}\right) \right). \quad (37)$$

Here,  $\mathcal{U}_N = \mathcal{N} \circ \mathcal{U}$ , and  $R(\theta, p)$  represents the resource robustness of the quantum state  $\frac{1}{2}(I + (1 - 2p)(\cos \theta X + \sin \theta Y))$ , given by

$$R(\theta, p) = \max \left\{ (2 - \sqrt{2}) \left( 1 + |1 - 2p| \cos \left( \theta - \frac{\pi}{4} \right) \right), 1 \right\}. \quad (38)$$

While the original bound in Ref. [38] was derived using resource robustness [61–64] of quantum channel, our key technical contribution in proving Theorem 5 is to show that the resource robustness for a noisy Pauli rotation gate  $\mathcal{N} \circ \mathcal{U}$  reduces to that of a single-qubit quantum state. This simplification is achieved by leveraging the symmetry inherent in the Choi state of  $\mathcal{N} \circ \mathcal{U}$ . For details and the proof of Theorem 5, we refer the reader to Appendix C.

For  $\theta = \pi/4$  and assuming  $\frac{p_z}{p_0 + p_z}, \frac{p_y}{p_x + p_y} < \frac{2 - \sqrt{2}}{4}$ , Eq. (37) simplifies to

$$F(\Theta_{\text{Clif}}^{\text{cor}}(\mathcal{U}_N), \mathcal{U}) \leq 1 - p_y - p_z. \quad (39)$$

This bound is achieved by applying the SCV gadget  $\Theta_{\mathcal{Q}_Z^{\text{cor}}}^{\text{cor}}$  to the noisy channel, with a Pauli-X operator used as feedback control. In this case, Pauli-X errors are corrected, while Pauli-Y errors are transformed into Pauli-Z errors. As a result, the noise channel is transformed into  $\Theta_{\mathcal{Q}_Z^{\text{cor}}}^{\text{cor}}(\mathcal{N})(\cdot) = (1 - p_y - p_z) \cdot + (p_y + p_z) Z \cdot Z$ , whose worst-case fidelity saturates the bound in Eq. (39). This result indicates that, even in the context of approximate purification of noisy channels, SCV under Pauli symmetry is an optimal protocol saturating the bound.

Besides showing the optimality of the SCV in noise purification, our result is also insightful from a resource-theoretic perspective. In fact, the bound in Theorem 5 holds for a much larger class of superchannels than the operationally motivated one that  $\Theta_{\text{Clif}}^{\text{cor}}$  belongs to. (See Appendix C for details.) Therefore, the tightness of the

bound in Theorem 5—and the original bound in Ref. [38] more broadly—with respect to operationally motivated classes of operations had been highly unclear. Our results demonstrate that it can indeed be achieved using an operationally motivated superchannel implemented by our SCV protocol. Thus, our findings highlight the practical relevance of resource theories in real-world scenarios.

## VII. DISCUSSION

In this work, we proposed symmetric channel verification (SCV) and its hardware-efficient variant, virtual symmetric channel verification (virtual SCV), as novel methods for purifying quantum channels by leveraging the symmetry inherent in quantum operations. These protocols generalize symmetry-based error countermeasures to the channel level, enabling noise reduction in scenarios where traditional symmetry verification [15, 16] is inapplicable, such as when input states or individual channels in a circuit lack shared symmetry.

SCV introduces a quantum phase estimation-like circuit that detects symmetry-breaking noise through coherent interactions with ancillary qubits. Virtual SCV provides a hardware-efficient alternative, requiring only a single-qubit ancilla and controlled Pauli gates, which are robust against noise. We demonstrated the effectiveness of SCV and virtual SCV in purifying quantum channels in various applications such as Hamiltonian simulation circuits and phase estimation circuits based on qubitization. Furthermore, we discussed their implementation in early fault-tolerant regimes, showing that SCV under Pauli symmetry represents an optimal protocol when operations are restricted to Clifford unitaries.

Our results highlight the versatility and practicality of SCV and virtual SCV as tools for noise reduction in quantum computation. Compared to traditional symmetry verification methods [15, 16] and their virtual variants [26–29], SCV and virtual SCV offer broader applicability by addressing noise in quantum channels with varying symmetries and input states that lack symmetry. In contrast to other channel purification protocols [17–24], SCV and virtual SCV require only a single noisy channel as input and make minimal assumptions about the target unitary. Consequently, our protocols are applicable to a wider range of scenarios and are easier to implement than existing methods.

Future research could explore several promising directions. First, while we focused on Hamiltonian simulation and phase estimation circuits as applications, our protocols can be applied to a wider range of tasks. One example worth exploring is the purification of noisy black-box unitaries under symmetry. In the setup of quantum amplitude amplification [65] or quantum metrology [60], we are given a black-box unitary, but we may know its symmetric structure beforehand. Our methods can be used to detect and correct errors in such black-box unitaries. Another interesting application is demonstrat-

ing quantum advantage using IQP circuits, which have been shown to be classically hard to simulate [66, 67]. Since IQP circuits possess a highly symmetric structure, our protocols can be straightforwardly applied to combat their noise.

Applications to quantum many-body physics can also be considered an important future direction. For example, in quench dynamics and dissipative dynamics, dynamical spontaneous symmetry breaking can occur, where the symmetry of the state is reduced compared to the symmetry of the time evolution channel itself [68]. When performing quantum simulations of such phenomena, it is crucial to precisely detect symmetry breaking arising from emergent phenomena itself but not that from the effect of noise. Therefore, SCV will play an important role in these simulations.

We can further explore the connection between channel purification and resource theory. In this work, we restricted our analysis to situations where the unitary operations constituting the purification gadget are Clifford gates. However, in general, allowing non-Clifford operations in the gadget is a natural extension, making it important to investigate the trade-off with magic-state consumption. Additionally, it is crucial to analyze resource utilization in fermionic and bosonic systems, as well as the convertibility of resources when utilizing hybrid quantum devices [69].

Finally, it is crucial to develop a fault-tolerant implementation of the SCV gadget. Even though noise in the SCV gadget may degrade its performance in detecting and correcting errors, the effect of such noise may be minimized by using flag qubits [70]. Developing a fault-tolerant implementation that is robust against such noise can further broaden the applicability of our protocols.

## ACKNOWLEDGEMENTS

The authors wish to thank Suguru Endo, Alvin Gonzales, and Yuki Koizumi, and Takahiro Sagawa for fruitful discussions. K.T. is supported by the Program for Leading Graduate Schools (MERIT-WINGS) and JST BOOST Grant Number JPMJBS2418. Y.M. is supported by JSPS KAKENHI Grant No. JP23KJ0421. R.T. is supported by JSPS KAKENHI Grant Number JP23K19028, JP24K16975, JST, CREST Grant Number JPMJCR23I3, Japan, MEXT KAKENHI Grant-in-Aid for Transformative Research Areas A “Extreme Universe” Grant Number JP24H00943. N.Y. is supported by JST PRESTO No. JPMJPR2119, JST Grant Number JPMJPF2221, JST CREST Grant Number JPMJCR23I4, IBM Quantum, JST ASPIRE Grant Number JPMJAP2316, JST ERATO Grant Number JPMJER2302, and Institute of AI and Beyond of the University of Tokyo.

## Appendix A: Proof of the main results

In this section, we provide detailed proofs of the theorems and corollaries stated in the main text, except Theorem 5.

### 1. Proof of Theorem 1

We begin with the proof of Theorem 1.

*Proof.* As discussed in the main text, we have

$$(\Theta_S^{\det}(\mathcal{U}_{\mathcal{N}}))(\cdot) = \sum_{ij} \Pi_i \mathcal{U}_{\mathcal{N}}(\Pi_i \cdot \Pi_j) \Pi_j. \quad (\text{A1})$$

Therefore, it suffices to show that  $\sum_{ij} \Pi_i \mathcal{U}_{\mathcal{N}}(\Pi_i \cdot \Pi_j) \Pi_j \propto \mathcal{U}$ . From the assumption  $\sum_i \Pi_i N_j \Pi_i \propto I_n$ , we have

$$\begin{aligned} \sum_{ij} \Pi_i \mathcal{U}_{\mathcal{N}}(\Pi_i \cdot \Pi_j) \Pi_j &= \sum_{ijk} \Pi_i N_k \mathcal{U}(\Pi_i \cdot \Pi_j) N_k^\dagger \Pi_j \\ &= \sum_{ijk} \Pi_i N_k \Pi_i \mathcal{U}(\cdot) \Pi_j N_k^\dagger \Pi_j \\ &\propto \mathcal{U}(\cdot), \end{aligned} \quad (\text{A2})$$

completing the proof.  $\square$

### 2. Proof of Corollary 1

Next, we proceed with the proof of Corollary 1.

*Proof.* From Theorem 1,  $\Theta_{\mathcal{Q}_U^{\text{com}}}^{\det}(\mathcal{U}_{\mathcal{N}}) = p_0 \mathcal{U}$  implies

$$\sum_j p_j \sum_{i_1 \dots i_r, i'_1 \dots i'_r} P_{j, i_1 \dots i_r} \mathcal{U}(\cdot) P_{j, i'_1 \dots i'_r} = p_0 \mathcal{U}(\cdot), \quad (\text{A3})$$

where  $P_{j, i_1 \dots i_r} = \Pi_{i_1}^1 \dots \Pi_{i_r}^r P_j \Pi_{i_r}^r \dots \Pi_{i_1}^1$  and  $\Pi_{i_k}^k = \frac{1}{2}(I_n + (-1)^{i_k} Q_k)$  represents the projector onto the eigenspace of  $Q_k$ . Since  $P_{j, i_1 \dots i_r}$  satisfies

$$\sum_{i_1 \dots i_r} P_{j, i_1 \dots i_r} = \begin{cases} P_j & (\forall k \in \{1, \dots, r\}, [P_j, Q_k] = 0), \\ 0 & (\text{otherwise}), \end{cases} \quad (\text{A4})$$

Eq. (A3) holds if and only if for all  $P_j \in \mathcal{P}_{\mathcal{N}}^{\det}$ , there exists a generator  $Q_k \in \mathcal{Q}_U^{\text{com}}$  that anti-commutes with  $P_j$ . Therefore, we obtain Eq. (16).

To derive Eq. (17), it suffices to show

$$P \notin \mathcal{Q}_U \Leftrightarrow \exists Q \in \mathcal{Q}_U^{\text{com}}, [P, Q] \neq 0. \quad (\text{A5})$$

To establish this equivalence, let us decompose  $\mathcal{Q}_U$  as

$$\mathcal{Q}_U = W^\dagger \left( \{I, X, Y, Z\}^{\otimes n_1} \otimes \{I, Z\}^{\otimes n_2} \otimes \{I\}^{\otimes n_3} \right) W, \quad (\text{A6})$$

where  $W$  is an  $n$ -qubit Clifford operator and  $n_1 + n_2 + n_3 = n$ . The existence of such a decomposition was established in Ref. [71]. Since  $\mathcal{Q}_U^{\text{com}}$  can also be represented as

$$\mathcal{Q}_U^{\text{com}} = \{Q \in \mathcal{P}_n \mid \forall P \in \mathcal{Q}_U, [P, Q] = 0\}, \quad (\text{A7})$$

we have

$$\mathcal{Q}_U^{\text{com}} = W^\dagger \left( \{I\}^{\otimes n_1} \otimes \{I, Z\}^{\otimes n_2} \otimes \{I, X, Y, Z\}^{\otimes n_3} \right) W. \quad (\text{A8})$$

Therefore,  $P \in \mathcal{Q}_U$  if and only if all  $Q \in \mathcal{Q}_U^{\text{com}}$  commute with  $P$ , establishing Eq. (A5).  $\square$

### 3. Proof of Theorem 2

Then, we provide the proof of Theorem 2.

*Proof.* Let  $U_E$  be the initial half of the SCV gadget  $\Theta_S^{\det}$  depicted in Fig. 2. Then, we have

$$U_E |\psi\rangle |0^m\rangle = \frac{1}{2^{m/2}} \sum_{jk} \exp\left[\frac{2\pi i}{2^m} jk\right] \Pi_j |\psi\rangle |k\rangle \quad (\text{A9})$$

for  $n$ -qubit quantum state  $|\psi\rangle$ . Using this  $U_E$  and some  $n+m$  qubit unitary  $U_D$ , we define a quantum superchannel  $\Theta_S^{\text{cor}}$  as in Eq. (3). Since  $U_E$  commutes with  $U$ , we have

$$\Theta_S^{\text{cor}}(\mathcal{U}_{\mathcal{N}}) = (\Theta_S^{\text{cor}}(\mathcal{N})) \circ \mathcal{U}. \quad (\text{A10})$$

Let us further define a codespace  $\mathcal{C}$  as a subspace of  $(n+m)$ -qubit system spanned by  $U_E |\psi\rangle |0^m\rangle$ , where  $|\psi\rangle$  is an arbitrary  $n$ -qubit quantum state. Then, from the quantum error correction condition [55, 56], there exists  $U_D$  such that  $\Theta_S^{\text{cor}}(\mathcal{N}) = \mathcal{I}$  if and only if for all  $n$ -qubit quantum state  $|\psi\rangle$  and  $|\phi\rangle$  and  $j, k \in \{0, \dots, K\}$ ,

$$\langle \psi | \langle 0^m | U_E^\dagger (N_j^\dagger N_k \otimes I_a) U_E |\phi\rangle |0^m\rangle = C_{ij} \langle \psi | \phi \rangle. \quad (\text{A11})$$

Here,  $C_{ij}$  is a complex number independent of  $|\psi\rangle$  and  $|\phi\rangle$  and  $\mathcal{I}$  is a identity channel on the  $n$ -qubit system.

From Eq. (A9), the LHS of Eq. (A11) can be represented as

$$\sum_i \langle \psi | \Pi_i N_j^\dagger N_k \Pi_i | \phi \rangle. \quad (\text{A12})$$

Therefore, Eq. (A11) is equivalent to

$$\sum_i \Pi_i N_j^\dagger N_k \Pi_i \propto I_n, \quad (\text{A13})$$

which completes the proof.  $\square$



#### 4. Proof of Corollary 2

Then, we proceed with the proof of Corollary 2.

*Proof.* From Theorem 2, for Pauli noise  $\mathcal{N}(\cdot) = \sum_{i=0}^K p_i P_i \cdot P_i$ , we have  $\Theta_{\mathcal{Q}_U^{\text{com}}}^{\text{or}}(\mathcal{U}_{\mathcal{N}}) = \mathcal{U}$  if and only if for all  $j, k \in \{0, \dots, K\}$ ,

$$\sum_{i_1 \dots i_r} \Pi_{i_1}^1 \cdots \Pi_{i_r}^r P_j P_k \Pi_{i_r}^r \cdots \Pi_{i_1}^1 \propto I_n, \quad (\text{A14})$$

where  $\Pi_{i_k}^k = \frac{1}{2}(I_n + (-1)^{i_k} Q_k)$ . For  $P_j P_k \neq I_n$ , Eq. (A14) holds if and only if there exists  $Q \in \mathcal{Q}_U^{\text{com}}$  that anti-commutes with  $P_j P_k$ . From Eq. (A5) in the proof of Corollary 1, this is equivalent to

$$\pm P_j P_k, \pm i P_j P_k \notin \mathcal{Q}_U. \quad (\text{A15})$$

Note that we have added a phase because  $P_j P_k$  may not be a Pauli operator in the set  $\mathcal{P}_n = \{I, X, Y, Z\}^{\otimes n}$  without the phase. Therefore, we arrive at the conclusion of Corollary 2.  $\square$

#### 5. Proof of Theorem 3

Then, we provide the proof of Theorem 3.

*Proof.* We first prove the necessary condition. Let us define a code space  $\mathcal{C}$  as a subspace of  $(n+m)$ -qubit system spanned by  $U_E |\psi\rangle |0^m\rangle$ , where  $|\psi\rangle$  is an arbitrary  $n$ -qubit quantum state. We define the stabilizer group of the code space  $\mathcal{C}$  as  $\mathcal{S} = U_E(\{I\}^{\otimes n} \otimes \{I, Z\}^{\otimes m}) U_E^\dagger$ , a set of logical Pauli operators as  $\bar{\mathcal{P}}_n = U_E(\mathcal{P}_n \otimes \{I\}^{\otimes m}) U_E^\dagger$ , and a set  $N(\mathcal{S}) = U_E(\mathcal{P}_n \otimes \{I, Z\}^{\otimes m}) U_E^\dagger$ . We also define sets with additional phase of  $\pm 1$  as  $\mathcal{S}^\pm = \{\pm 1\} \cdot \mathcal{S}$  and  $N(\mathcal{S})^\pm = \{\pm 1\} \cdot N(\mathcal{S})^\pm$ . Note that  $N(\mathcal{S})^\pm = \bar{\mathcal{P}}_n \cdot \mathcal{S}^\pm = \{\pm 1\} \cdot \{P \in \mathcal{P}_{n+m} \mid \forall Q \in \mathcal{S}, [P, Q] = 0\}$ .

When we set  $\theta = 0$ , we have

$$\Theta_{\text{Clif}}^{\text{det}}(\mathcal{N}_{P_i}) = \delta_{i0} \mathcal{I}_n. \quad (\text{A16})$$

This means that the code space  $\mathcal{C}$  can detect the set of errors  $\{P_i \otimes I^{\otimes m}\}_{i=1}^K$ . Therefore, from the quantum error detection condition [55, 56], we obtain

$$\forall P_i \in \mathcal{P}_n^{\text{det}}, P_i \otimes I^{\otimes m} \notin N(\mathcal{S})^\pm \setminus \mathcal{S}^\pm. \quad (\text{A17})$$

When we consider the case where the error did not occur, we have

$$\Theta_{\text{Clif}}^{\text{det}}(\mathcal{U}) = \mathcal{U}. \quad (\text{A18})$$

For  $\theta = 0$ , this means

$$U_D U_E |\psi\rangle |0^m\rangle = |\psi\rangle |0^m\rangle \quad (\text{A19})$$

for all input state  $|\psi\rangle$ . In other words,

$$U_D U_E (I^{\otimes n} \otimes |0^m\rangle\langle 0^m|) = I^{\otimes n} \otimes |0^m\rangle\langle 0^m|, \quad (\text{A20})$$

so the Clifford unitary  $U_D$  satisfies

$$U_E (I^{\otimes n} \otimes |0^m\rangle\langle 0^m|) = U_D^\dagger (I^{\otimes n} \otimes |0^m\rangle\langle 0^m|). \quad (\text{A21})$$

By combining Eq. (A18) with Eq. (A21), we obtain

$$\begin{aligned} & (I^{\otimes n} \otimes |0^m\rangle\langle 0^m|) U_E^\dagger (e^{i\theta H} \otimes I^{\otimes m}) U_E (I^{\otimes n} \otimes |0^m\rangle\langle 0^m|) \\ &= (e^{i\theta H} \otimes |0^m\rangle\langle 0^m|). \end{aligned} \quad (\text{A22})$$

When we differentiate this equation by  $\theta$  and substituting  $\theta = 0$ , we have

$$\begin{aligned} & (I^{\otimes n} \otimes |0^m\rangle\langle 0^m|) U_E^\dagger (H \otimes I^{\otimes m}) U_E (I^{\otimes n} \otimes |0^m\rangle\langle 0^m|) \\ &= (H \otimes |0^m\rangle\langle 0^m|). \end{aligned} \quad (\text{A23})$$

By sandwiching this equality with  $U_E$  and  $U_E^\dagger$ , we obtain

$$\Pi (H \otimes I^{\otimes m}) \Pi = \Pi \bar{H} \Pi, \quad (\text{A24})$$

where  $\Pi = U_E (I^{\otimes n} \otimes |0^m\rangle\langle 0^m|) U_E^\dagger$  is the projector to the code space  $\mathcal{C}$  and  $\bar{H} = U_E (H \otimes I^{\otimes m}) U_E^\dagger$  is the logical  $H$  operator on  $\mathcal{C}$ .

Let us decompose the Hamiltonian  $H$  using Pauli operator  $Q_i \in \mathcal{P}_n$  as  $H = \sum_{i=1}^A h_i Q_i$ , where  $h_i \neq 0$ . Then, from Eq. (A24), we have

$$\sum_{i=1}^A h_i \Pi (Q_i \otimes I^{\otimes m}) \Pi = \sum_{i=1}^A h_i \Pi \bar{Q}_i \Pi, \quad (\text{A25})$$

where  $\bar{Q}_i = U_E (Q_i \otimes I^{\otimes m}) U_E^\dagger \in \bar{\mathcal{P}}_n$  is the logical  $Q_i$  operator on the code space  $\mathcal{C}$ . Since the number of Pauli terms in RHS and LHS of Eq. (A25) are both  $A$ ,  $Q_i \otimes I^{\otimes m}$  should be a logical Pauli operator on the code space  $\mathcal{C}$ . Therefore, there exists  $S_1, \dots, S_A \in \mathcal{S}^\pm$  such that

$$\{Q_i \otimes I^{\otimes m}\}_{i=1}^A = \{\bar{Q}_i S_i\}_{i=1}^A. \quad (\text{A26})$$

When we consider the set of Pauli operators generated from this set, we have

$$\mathcal{Q}_H \otimes \{I^{\otimes m}\} \subset \bar{\mathcal{P}}_n \cdot \mathcal{S}^\pm = N(\mathcal{S})^\pm. \quad (\text{A27})$$

Here, the definition of  $\mathcal{Q}_H$  is given in Eq. (13). Let us assume that there exists  $Q \in \mathcal{Q}_H \setminus \{I^{\otimes n}\}$  such that  $Q \otimes I^{\otimes m} = S \in \mathcal{S}^\pm$ . In this case, we can show that  $|\mathcal{Q}_H| \geq |\mathcal{Q}_H| + 1$ , which is a contradiction. To show this, let us define the logical version of the set  $\mathcal{Q}_H$  as  $\bar{\mathcal{Q}}_H = U_E (\mathcal{Q}_H \otimes I^{\otimes m}) U_E^\dagger \subset \bar{\mathcal{P}}_n$ . Then, from Eq. (A26), for all  $\bar{Q}' \in \bar{\mathcal{Q}}_H$ , there exists different  $Q'' \in \mathcal{Q}_H$  such that  $Q'' \otimes I^{\otimes m} = \bar{Q}' S'$  for some stabilizer  $S' \in \mathcal{S}^\pm$ . However, under the assumption of the existence of  $Q \otimes I^{\otimes m} = S \neq I^{\otimes(n+m)}$ , there exists at least two different  $Q'' \in \mathcal{Q}_H$  for  $\bar{Q}' = I^{\otimes n+m}$ . This means  $|\mathcal{Q}_H| \geq |\bar{\mathcal{Q}}_H| + 1 = |\mathcal{Q}_H| + 1$ , so we have  $(\mathcal{Q}_H \otimes \{I^{\otimes m}\}) \setminus \{I^{\otimes(n+m)}\} \cap \mathcal{S}^\pm = \emptyset$ . Thus, we obtain

$$(\mathcal{Q}_H \setminus \{I^{\otimes n}\}) \otimes \{I^{\otimes m}\} \subset N(\mathcal{S})^\pm \setminus \mathcal{S}^\pm. \quad (\text{A28})$$

By combining Eq. (A17) and (A28), we obtain

$$\forall P_i \in \mathcal{P}_N^{\text{det}}, P_i \notin \mathcal{Q}_H \setminus \{I^{\otimes n}\}, \quad (\text{A29})$$

which is equivalent to

$$\mathcal{P}_N^{\text{det}} \cap \mathcal{Q}_H = \emptyset. \quad (\text{A30})$$

For the sufficiency, we use SCV gadget  $\Theta_{\mathcal{Q}_H^{\text{com}}}^{\text{det}}$ . From Corollary 1,  $\Theta_{\mathcal{Q}_H^{\text{com}}}^{\text{det}}$  can be used to detect errors satisfying Eq. (30).  $\square$

## 6. Proof of Theorem 4

Finally, we prove Theorem 4.

*Proof.* We first prove the necessary condition. As in the proof of Theorem 3, let us define a code space  $\mathcal{C}$  as a subspace of  $(n+m)$ -qubit system spanned by  $U_E |\psi\rangle |0^m\rangle$ , where  $|\psi\rangle$  is an arbitrary  $n$ -qubit quantum state. We define the stabilizer group of the code space  $\mathcal{C}$  as  $\mathcal{S} = U_E(\{I\}^{\otimes n} \otimes \{I, Z\}^{\otimes m})U_E^\dagger$ , a set of logical Pauli operators as  $\bar{\mathcal{P}}_n = U_E(\mathcal{P}_n \otimes \{I\}^{\otimes m})U_E^\dagger$ , and a set  $N(\mathcal{S}) = U_E(\mathcal{P}_n \otimes \{I, Z\}^{\otimes m})U_E^\dagger$ . We also define sets with additional phase of  $\pm 1$  as  $\mathcal{S}^\pm = \{\pm 1\} \cdot \mathcal{S}$  and  $N(\mathcal{S})^\pm = \{\pm 1\} \cdot N(\mathcal{S})^\pm$ . Note that  $N(\mathcal{S})^\pm = \bar{\mathcal{P}}_n \cdot \mathcal{S}^\pm = \{\pm 1\} \cdot \{P \in \mathcal{P}_{n+m} \mid \forall Q \in \mathcal{S}, PQ = QP\}$ .

When we set  $\theta = 0$ , we have

$$\Theta_{\text{Clif}}^{\text{cor}}(\mathcal{N}) = \mathcal{I}, \quad (\text{A31})$$

where  $\mathcal{I}$  is an identity operator of an  $n$ -qubit system. This means that the codespace  $\mathcal{C}$  can correct the noise  $\mathcal{N} \otimes \mathcal{I}_a(\cdot) = \sum_{i=0}^K p_i (P_i \otimes I^{\otimes m}) \cdot (P_i \otimes I^{\otimes m})$ . Therefore, from the quantum error correction condition [55, 56], we obtain

$$\forall P \in \mathcal{P}_N^{\text{cor}}, P \otimes I^{\otimes m} \notin N(\mathcal{S})^\pm \setminus \mathcal{S}^\pm. \quad (\text{A32})$$

Since no error occurs with probability  $p_0 \neq 0$ , we have

$$\Theta_{\text{Clif}}^{\text{cor}}(\mathcal{U}) = \mathcal{U}. \quad (\text{A33})$$

For  $\theta = 0$ , this means

$$U_D U_E |\psi\rangle |0^m\rangle = |\psi\rangle |\alpha\rangle \quad (\text{A34})$$

for all input state  $|\psi\rangle$ , where  $|\alpha\rangle$  is a  $m$ -qubit quantum state independent of  $|\psi\rangle$ . Since the operation performed on the ancilla does not affect the system qubits, we can modulate  $U_D$  so that  $|\alpha\rangle = |0^m\rangle$ . In this case, we have

$$(I^{\otimes n} \otimes |0^m\rangle\langle 0^m|)U_D U_E = I^{\otimes n} \otimes |0^m\rangle\langle 0^m|, \quad (\text{A35})$$

so the Clifford unitary  $U_D$  satisfies

$$U_E(I^{\otimes n} \otimes |0^m\rangle\langle 0^m|) = U_D^\dagger(I^{\otimes n} \otimes |0^m\rangle\langle 0^m|). \quad (\text{A36})$$

From Eq. (A33) and Eq. (A36), when we consider post-selecting measurement results instead of discarding them, we obtain

$$(I^{\otimes n} \otimes |0^m\rangle\langle 0^m|)U_E^\dagger(e^{i\theta H} \otimes I^{\otimes m})U_E(I^{\otimes n} \otimes |0^m\rangle\langle 0^m|) \propto (e^{i\theta H} \otimes |0^m\rangle\langle 0^m|). \quad (\text{A37})$$

Then, in the same way as in the proof of Theorem 3, we obtain

$$((\mathcal{Q}_H) \setminus \{I^{\otimes n}\}) \otimes \{I^{\otimes m}\} \subset N(\mathcal{S})^\pm \setminus \mathcal{S}^\pm. \quad (\text{A38})$$

By combining Eq. (A32) and (A38), we obtain

$$\forall P \in \mathcal{P}_N^{\text{cor}}, P \notin \mathcal{Q}_H \setminus \{I^{\otimes n}\}, \quad (\text{A39})$$

which is equivalent to

$$\mathcal{P}_N^{\text{cor}} \cap \mathcal{Q}_H = \emptyset. \quad (\text{A40})$$

For the sufficiency, we use SCV gadget  $\Theta_{\mathcal{Q}_H^{\text{com}}}^{\text{cor}}$ . From Theorem 4, this can be used to detect errors satisfying Eq. (27).  $\square$

## Appendix B: SELECT operation of the 2D Fermi-Hubbard model on a square lattice

In this section, we explain the SELECT operation for the 2D Fermi-Hubbard model on a square lattice with linear system size  $M$  and system qubit count  $n = 2M^2$ , which we have used to demonstrate the performance of virtual SCV in Sec. IV C. The Hamiltonian of the Fermi-Hubbard model is given by

$$H = -t \sum_{\langle p,q \rangle, \sigma} a_{p,\sigma}^\dagger a_{q,\sigma} + \frac{u}{2} \sum_{p, \alpha \neq \beta} n_{p,\alpha} n_{p,\beta}, \quad (\text{B1})$$

where  $a_{p,\sigma}^{(\dagger)}$  indicates the fermionic annihilation (creation) operator on the site  $p$  with spin  $\sigma$ ,  $t$  is the hopping amplitude, and  $u$  is the magnitude of onsite interaction. Here, the summation  $\sum_{\langle p,q \rangle}$  runs over adjacent pairs on a square lattice under periodic boundary conditions.

Under the Jordan-Wigner transformation, this Hamiltonian is mapped to a qubit Hamiltonian as

$$H = -\frac{t}{2} \sum_{\langle p,q \rangle, \sigma} \left( X_{p,\sigma} \vec{Z} X_{q,\sigma} + Y_{p,\sigma} \vec{Z} Y_{q,\sigma} \right) + \frac{u}{8} \sum_{p, \alpha \neq \beta} Z_{p,\alpha} Z_{p,\beta} - \frac{u}{4} \sum_{p,\sigma} Z_{p,\sigma}, \quad (\text{B2})$$

where we have neglected the constant shift of energy. Also, the notation  $\vec{Z}$  indicates the so-called ‘‘Z-string.’’ Namely,  $X_{p,\sigma} \vec{Z} X_{q,\sigma}$  is a product of Pauli X operators and Pauli Z operators whose indices run between integers that are used to uniquely label the pairs  $(p, \sigma)$  and  $(q, \sigma)$ .

As proposed in Ref. [31], the SELECT operation for this Hamiltonian can be implemented by the circuit shown in

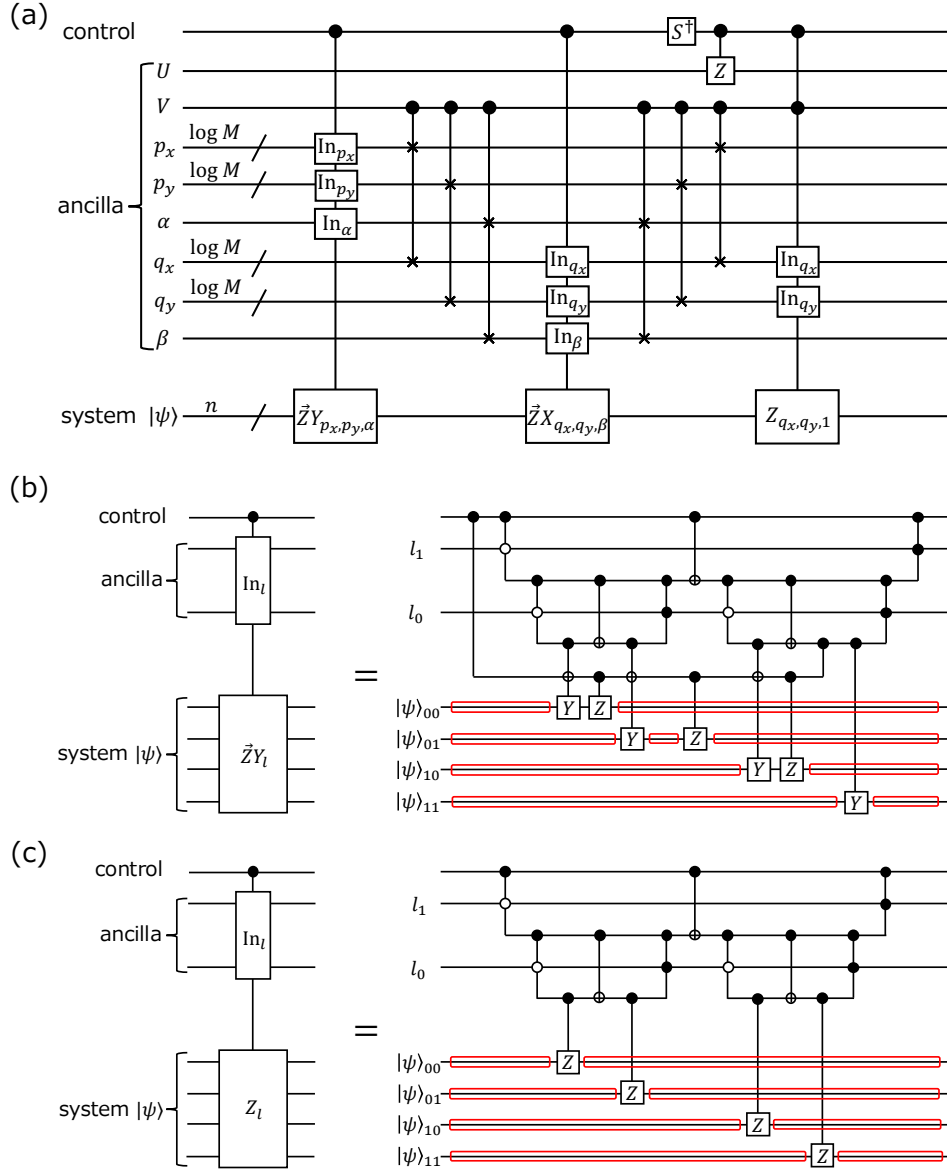


FIG. 10. **SELECT** operation of the 2D Fermi-Hubbard model on a square lattice with linear system size  $M$  and system qubit count  $n = 2M^2$  that use the adder to iterate the indices of ancilla [31, 72]. Panel (a) represents the entire circuit, while Panels (b) and (c) represent the sub-circuits shown in Panel (a). The system qubits include many idling qubits, illustrated in red. Idling errors occurring here can be mitigated using virtual SCV. Note that  $\text{In}_l$  indicates that the operation is controlled by  $l$ -th computational basis of ancilla system,  $p_x, p_y, q_x$  and  $q_y$  denote the two-dimensional site indices,  $\alpha$  and  $\beta$  indicate the spin of fermions, and  $U$  and  $V$  are introduced to discriminate between  $Z$  and  $ZZ$  contribution to the Hamiltonian [31].

Fig. 10. As illustrated in red, the system qubits include many idling qubits. By applying virtual SCV to these red idling qubits, idling errors can be mitigated, as discussed in Sec. IV C.

### Appendix C: Resource-Theoretic Analysis on the Limitations of Channel Purification

In this section, we provide the proof of Theorem 5 by employing the fundamental tools of the dynamical resource theory of magic [38, 64, 73]. The resource theory of magic [74] is the framework that allows us to quantitatively analyze the property of the states that cannot be prepared by a stabilizer operation. Stabilizer operations are operations consisting of (i) preparing states  $|0\rangle$ ,

(ii) applying Clifford unitaries, (iii) measuring with computational basis, and (iv) applying the above operations conditioned on the measurement outcomes and classical randomness. The set of states that can be prepared by stabilizer operations are called stabilizer states, and it coincides with the probabilistic mixture of pure states prepared by Clifford unitaries.

Let  $\mathbb{F}$  denote the set of stabilizer states of arbitrary qubit counts. In resource-theoretic analysis, one considers the set of operations accessible in the given operational setting. In the case of the magic resource theory, the most operational choice is to take the set of stabilizer operations as such freely available operations. However, the set of stabilizer operations is theoretically hard to deal with because of its complex mathematical structure. It turns out that it is useful to consider a larger set of operations that contains stabilizer operations as a subset. The standard choice is to consider the set of completely stabilizer-preserving channels defined by

$$\mathbb{O} = \{\mathcal{E} \in \text{CPTP} \mid \forall m \in \mathbb{N}, \forall \sigma \in \mathbb{F}, \mathcal{E} \otimes \mathcal{I}_m(\sigma) \in \mathbb{F}\}, \quad (\text{C1})$$

where CPTP denotes the set of completely positive trace-preserving (CPTP) maps, and  $\mathcal{I}_m$  represents the identity channel on an  $m$ -qubit system. The advantage of considering this set of operations is that it can be concisely characterized by looking at the magic property of their Choi states. Namely, it is known that a channel  $\mathcal{E}$  is completely stabilizer-preserving if and only if its Choi state  $J_{\mathcal{E}} = \mathcal{E} \otimes \mathcal{I}(|\Psi\rangle\langle\Psi|)$  is a stabilizer state [64]:

$$\mathbb{O} = \{\mathcal{E} \in \text{CPTP} \mid J_{\mathcal{E}} \in \mathbb{F}\}. \quad (\text{C2})$$

Here,  $|\Psi\rangle = 2^{-n/2} \sum_i |i\rangle |i\rangle$  is the maximally entangled state with  $\{|i\rangle\}$  being a computational basis, and  $\mathcal{I}$  is the identity channel of the same dimension.

Toward the application to our setting of SCV, we now extend this framework to the dynamical resource theory of magic, where we consider the transformation of quantum channels by available processes. In general, the transformation of quantum channels is realized by quantum superchannels [75, 76], which can be implemented by applying pre- and post-processing channels before and after the given channel. The dynamical resource theory allows us to analyze the consequence of limiting the available superchannels.

In the setting discussed in Sec. VI, the allowed set of superchannels consists of pre- and post-processing Clifford unitaries followed by the partial trace, represented as

$$\Theta_{\text{Clif}}^{\text{cor}}(\mathcal{E}) : \rho \mapsto \text{tr}_a[\mathcal{U}_D \circ (\mathcal{E} \otimes \mathcal{I}_a) \circ \mathcal{U}_E(\rho \otimes |0^m\rangle\langle 0^m|)], \quad (\text{C3})$$

where  $\mathcal{U}_E$  and  $\mathcal{U}_D$  are Clifford unitary channels and  $\mathcal{I}_a$  is the identity channel on arbitrary dimension. One can easily check that these superchannels surely preserve the set of completely stabilizer-preserving channels—if we sandwich an arbitrary channel in  $\mathbb{O}$  by Clifford unitaries, then the resulting channel after the partial trace is also

in  $\mathbb{O}$ . This means that if we consider the set of stabilizer-preserving superchannels defined by

$$\mathbb{S} = \{\Theta \in \text{superchannel} \mid \forall \mathcal{E} \in \mathbb{O}, \Theta(\mathcal{E}) \in \mathbb{O}\}, \quad (\text{C4})$$

the superchannel  $\Theta_{\text{Clif}}^{\text{cor}}$  of the form (C3) considered in Sec. VI are included in  $\mathbb{S}$ . This implies that, while the set  $\mathbb{S}$  is strictly larger than the set of superchannels  $\Theta_{\text{Clif}}^{\text{cor}}$  constructed from Clifford unitaries, limitations on channel purification using axiomatic superchannels  $\Theta \in \mathbb{S}$  also impose fundamental limitations on such operationally motivated superchannels  $\Theta_{\text{Clif}}^{\text{cor}}$ . Therefore, we derive the fundamental limits of channel purification using stabilizer-preserving superchannels  $\Theta \in \mathbb{S}$ .

To achieve this, we employ the resource robustness  $R_{\mathbb{F}}(\rho)$  [61, 62] and resource weight  $W_{\mathbb{F}}(\rho)$  [77, 78] of a quantum state  $\rho$ , defined as

$$R_{\mathbb{F}}(\rho) = \min \{\lambda \geq 1 \mid \exists \sigma \in \mathbb{F}, \rho \leq \lambda \sigma\}, \quad (\text{C5})$$

$$W_{\mathbb{F}}(\rho) = \max \{\lambda \leq 1 \mid \exists \sigma \in \mathbb{F}, \rho \geq \lambda \sigma\}. \quad (\text{C6})$$

Similarly, we define the resource robustness  $R_{\mathbb{O}}(\mathcal{E})$  [63, 79] and resource weight  $W_{\mathbb{O}}(\mathcal{E})$  [78] of a quantum channel  $\mathcal{E}$  as

$$R_{\mathbb{O}}(\mathcal{E}) = \min \{\lambda \geq 1 \mid \exists \mathcal{M} \in \mathbb{O}, J_{\mathcal{E}} \leq \lambda J_{\mathcal{M}}\}, \quad (\text{C7})$$

$$W_{\mathbb{O}}(\mathcal{E}) = \max \{\lambda \leq 1 \mid \exists \mathcal{M} \in \mathbb{O}, J_{\mathcal{E}} \geq \lambda J_{\mathcal{M}}\}. \quad (\text{C8})$$

These measures quantify how far a quantum state  $\rho$  and a quantum channel  $\mathcal{E}$  deviate from the sets of stabilizer states  $\mathbb{F}$  and completely stabilizer-preserving channels  $\mathbb{O}$ , respectively. Additionally, we introduce the fidelity-based measure

$$F_{\mathbb{O}}(\mathcal{E}) = \max_{\mathcal{M} \in \mathbb{O}} F(\mathcal{E}, \mathcal{M}), \quad (\text{C9})$$

where  $F(\mathcal{E}, \mathcal{M})$  is the worst-case fidelity defined in Eq. (36).

Using these resource measures, Ref. [38] derived an upper bound on the worst-case fidelity achievable through channel purification with stabilizer-preserving superchannels  $\Theta \in \mathbb{S}$ :

**Lemma 1.** (*Theorem 1 of Ref. [38]*) *Let  $\mathcal{U}$  be a unitary channel, and let  $\mathcal{U}_{\mathcal{N}} = \mathcal{N} \circ \mathcal{U}$  be a noisy channel affected by a noise channel  $\mathcal{N}$ . Then, the worst-case fidelity between the ideal channel  $\mathcal{U}$  and the purified noisy channel  $\Theta(\mathcal{U}_{\mathcal{N}})$  under a stabilizer-preserving superchannel  $\Theta \in \mathbb{S}$  is upper bounded as*

$$F(\Theta(\mathcal{U}_{\mathcal{N}}), \mathcal{U}) \leq F_{\mathbb{O}}(\mathcal{U}) R_{\mathbb{O}}(\mathcal{U}_{\mathcal{N}}), \quad (\text{C10})$$

$$F(\Theta(\mathcal{U}_{\mathcal{N}}), \mathcal{U}) \leq 1 - (1 - F_{\mathbb{O}}(\mathcal{U})) W_{\mathbb{O}}(\mathcal{U}_{\mathcal{N}}). \quad (\text{C11})$$

We remark that (C11) was also shown in Ref. [73]. Lemma 1 ensures that, if we can evaluate the resource measures  $R_{\mathbb{O}}(\mathcal{U}_{\mathcal{N}})$ ,  $W_{\mathbb{O}}(\mathcal{U}_{\mathcal{N}})$ , and  $F_{\mathbb{O}}(\mathcal{U})$ , we can derive an upper bound on the worst-case fidelity. However, analytical computation of these measures is usually not feasible. The examples known to come with analytical expressions have been limited to the case of the channels

implementable by gate teleportation with a magic state, where the magic measures for channels can be reduced to those of the corresponding magic states [38]. The channel  $\mathcal{U}_{\mathcal{N}}$  of our interest is generally not in such a class, preventing us from directly applying the previous approach.

Here, we present a new approach to computing these resource measures and obtain analytical expressions for an operationally important class of noisy unitary channels. To this end, we consider the Pauli-Z rotation gate  $\mathcal{U}(\cdot) = e^{-i\frac{\theta}{2}Z} \cdot e^{i\frac{\theta}{2}Z}$  under single-qubit Pauli noise  $\mathcal{N}(\cdot) = p_0 \cdot + p_x X \cdot X + p_y Y \cdot Y + p_z Z \cdot Z$ . In this case, as shown in the following lemma, the resource robustness and resource weight for quantum channels can be reduced to that of a quantum state:

**Lemma 2.** *Let  $\mathcal{U}(\cdot) = e^{-i\frac{\theta}{2}Z} \cdot e^{i\frac{\theta}{2}Z}$  be a Pauli-Z rotation gate with  $0 \leq \theta \leq \pi/4$ , and let  $\mathcal{U}_{\mathcal{N}} = \mathcal{N} \circ \mathcal{U}$  be a noisy channel affected by single-qubit Pauli noise  $\mathcal{N}(\cdot) = p_0 \cdot + p_x X \cdot X + p_y Y \cdot Y + p_z Z \cdot Z$ . Then, the resource robustness and the resource weight of the noisy channel  $\mathcal{U}_{\mathcal{N}}$  is given by*

$$R_{\mathbb{O}}(\mathcal{U}_{\mathcal{N}}) = (p_0 + p_z)R\left(\theta, \frac{p_z}{p_0 + p_z}\right) + (p_x + p_y)R\left(\theta, \frac{p_y}{p_x + p_y}\right), \quad (\text{C12})$$

$$W_{\mathbb{O}}(\mathcal{U}_{\mathcal{N}}) = (p_0 + p_z)W\left(\theta, \frac{p_z}{p_0 + p_z}\right) + (p_x + p_y)W\left(\theta, \frac{p_y}{p_x + p_y}\right). \quad (\text{C13})$$

Here,  $R(\theta, p)$  and  $W(\theta, p)$  represents the resource robustness and the resource weight of the quantum state  $\rho(\theta, p) = \frac{1}{2}(I + (1 - 2p)(\cos \theta X + \sin \theta Y))$ , given by

$$R(\theta, p) = \max \left\{ 1, \frac{\sqrt{2} + x + y}{\sqrt{2} + 1} \right\}, \quad (\text{C14})$$

$$W(\theta, p) = \min \left\{ 1, \frac{\sqrt{2} - (x + y)}{\sqrt{2} - 1}, \frac{1 - (x^2 + y^2)}{2(1 - x)} \right\}, \quad (\text{C15})$$

where  $x = |1 - 2p| \cos \theta$  and  $y = |1 - 2p| \sin \theta$ .

*Proof.* Since the proof for the resource weight is essentially the same as that for the resource robustness, we concentrate on the proof for the resource robustness. Moreover, Eq. (C14) can be obtained by analyzing the constrained optimization problem Eq. (C5) geometrically using the Bloch sphere, which can be checked to coincide with the value obtained from a general formula shown in Proposition 5 of Ref. [80]. Therefore, we aim at showing Eq. (C12).

From Eq. (C2) and Eq. (C7), resource robustness  $R_{\mathbb{O}}(\mathcal{U}_{\mathcal{N}})$  can be represented as

$$R_{\mathbb{O}}(\mathcal{U}_{\mathcal{N}}) = \min \{ \lambda \geq 1 \mid \exists \sigma \in \mathbb{F}, \text{tr}_S[\sigma] = I/2, J_{\mathcal{U}_{\mathcal{N}}} \leq \lambda \sigma \}. \quad (\text{C16})$$

Here,  $\text{tr}_S$  represents the partial trace over the subspace where  $\mathcal{U}_{\mathcal{N}}$  acts, and  $\text{tr}_S[\sigma] = I/2$  represents the trace-preserving condition of the channel  $\mathcal{M} \in \mathbb{O}$ . Since the maximally entangled state can be represented as

$$|\Psi\rangle\langle\Psi| = \Pi_0 \rho_L(0, 0) \Pi_0, \quad (\text{C17})$$

where  $\Pi_i = \frac{1}{2}(II + (-1)^i ZZ)$  is the projector onto the eigenspace of  $ZZ$  with eigenvalue  $(-1)^i$  and  $\rho_L(\theta, p) = \frac{1}{2}(II + (1 - 2p)(\cos \theta XX + \sin \theta YX))$ , the Choi state  $J_{\mathcal{U}_{\mathcal{N}}}$  can be expressed as

$$J_{\mathcal{U}_{\mathcal{N}}} = (p_0 + p_z) \Pi_0 \rho_L\left(\theta, \frac{p_z}{p_0 + p_z}\right) \Pi_0 + (p_x + p_y) \Pi_1 \rho_L\left(-\theta, \frac{p_y}{p_x + p_y}\right) \Pi_1. \quad (\text{C18})$$

We note that  $\Pi_i \rho_L(\theta, p) \Pi_i$  can be interpreted as a logical state on the  $n = 2$  repetition code, where the quantum state  $\rho(\theta, p) = \frac{1}{2}(I + (1 - 2p)(\cos \theta X + \sin \theta Y))$  is encoded. Below, we denote  $q_0 = p_0 + p_z$ ,  $q_1 = p_x + p_y$ ,  $\rho_0 = \rho(\theta, \frac{p_z}{p_0 + p_z})$ ,  $\rho_1 = \rho(-\theta, \frac{p_y}{p_x + p_y})$ ,  $\rho_{0,L} = \rho_L(\theta, \frac{p_z}{p_0 + p_z})$  and  $\rho_{1,L} = \rho_L(-\theta, \frac{p_y}{p_x + p_y})$  for simplicity. Under this notation, we have

$$J_{\mathcal{U}_{\mathcal{N}}} = q_0 \Pi_0 \rho_{0,L} \Pi_0 + q_1 \Pi_1 \rho_{1,L} \Pi_1. \quad (\text{C19})$$

For single-qubit quantum state  $\rho_i$  and the corresponding logical state  $\Pi_i \rho_{i,L} \Pi_i$ , let us show

$$R_{\mathbb{F}}(\Pi_i \rho_{i,L} \Pi_i) = R_{\mathbb{F}}(\rho_i). \quad (\text{C20})$$

The essential point is that for any single-qubit quantum state  $\sigma_i$  and the corresponding logical state  $\Pi_i \sigma_{i,L} \Pi_i$ , two inequalities

$$\rho_i \leq \lambda \sigma_i, \quad (\text{C21})$$

$$\Pi_i \rho_{i,L} \Pi_i \leq \lambda \Pi_i \sigma_{i,L} \Pi_i \quad (\text{C22})$$

are equivalent. Therefore, it is sufficient to show that the optimality in Eq. (C5) can be achieved with a logical state  $\Pi_i \sigma_{i,L} \Pi_i$  belonging to the  $(-1)^i$  eigenspace of  $ZZ$ . Let  $\sigma_{i,\text{opt}} \in \mathbb{F}$  be a 2-qubit stabilizer state satisfying  $\Pi_i \rho_{i,L} \Pi_i \leq R_{\mathbb{F}}(\Pi_i \rho_{i,L} \Pi_i) \sigma_{i,\text{opt}}$ . Then, by sandwiching this state with  $\Pi_i$ , we obtain

$$\Pi_i \rho_{i,L} \Pi_i \leq R_{\mathbb{F}}(\Pi_i \rho_{i,L} \Pi_i) \text{tr}[\Pi_i \sigma_{i,\text{opt}} \Pi_i] \frac{\Pi_i \sigma_{i,\text{opt}} \Pi_i}{\text{tr}[\Pi_i \sigma_{i,\text{opt}} \Pi_i]}. \quad (\text{C23})$$

Since  $\frac{\Pi_i \sigma_{i,\text{opt}} \Pi_i}{\text{tr}[\Pi_i \sigma_{i,\text{opt}} \Pi_i]} \in \mathbb{F}$ , we have  $\text{tr}[\Pi_i \sigma_{i,\text{opt}} \Pi_i] = 1$  from the definition of  $R_{\mathbb{F}}(\Pi_i \rho_{i,L} \Pi_i)$ . This implies  $\sigma_{i,\text{opt}} = \Pi_i \sigma_{i,\text{opt}} \Pi_i$ , meaning that the optimal state  $\sigma_{i,\text{opt}}$  is always a logical state belonging to the  $(-1)^i$  eigenspace of  $ZZ$ . Therefore, we have Eq. (C20). We note that the optimal state  $\sigma_i \in \mathbb{F}$  achieving  $\rho_i \leq R_{\mathbb{F}}(\rho) \sigma_i$  lies on the  $xy$ -plane within the Bloch sphere. Therefore, the optimal state  $\Pi_i \sigma_{i,L} \Pi_i \in \mathbb{F}$  satisfying  $\Pi_i \rho_{i,L} \Pi_i \leq R_{\mathbb{F}}(\Pi_i \rho_{i,L} \Pi_i) \Pi_i \sigma_{i,L} \Pi_i$  can be represented as

$$\Pi_i \sigma_{i,L} \Pi_i = \Pi_i \frac{1}{2}(II + x_i XX + y_i YX) \Pi_i \quad (\text{C24})$$

for some  $x_i, y_i \in \mathbb{R}$ .

Next, let us show

$$R_{\mathbb{F}}(J_{\mathcal{U}_{\mathcal{N}}}) = q_0 R_{\mathbb{F}}(\rho_0) + q_1 R_{\mathbb{F}}(\rho_1). \quad (\text{C25})$$

Let  $\sigma_{\text{opt}} \in \mathbb{F}$  be a 2-qubit stabilizer state satisfying  $J_{\mathcal{U}_{\mathcal{N}}} \leq R_{\mathbb{F}}(J_{\mathcal{U}_{\mathcal{N}}})\sigma_{\text{opt}}$ . By sandwiching this inequality with  $\Pi_i$ , we obtain

$$q_i \Pi_i \rho_{i,L} \Pi_i \leq R_{\mathbb{F}}(J_{\mathcal{U}_{\mathcal{N}}}) \text{tr}[\Pi_i \sigma_{\text{opt}} \Pi_i] \frac{\Pi_i \sigma_{\text{opt}} \Pi_i}{\text{tr}[\Pi_i \sigma_{\text{opt}} \Pi_i]}. \quad (\text{C26})$$

Since  $\frac{\Pi_i \sigma_{\text{opt}} \Pi_i}{\text{tr}[\Pi_i \sigma_{\text{opt}} \Pi_i]} \in \mathbb{F}$ , this inequality implies

$$R_{\mathbb{F}}(J_{\mathcal{U}_{\mathcal{N}}}) \text{tr}[\Pi_i \sigma_{\text{opt}} \Pi_i] \geq q_i R_{\mathbb{F}}(\Pi_i \rho_{i,L} \Pi_i) = q_i R_{\mathbb{F}}(\rho_i), \quad (\text{C27})$$

where we use Eq. (C20). Since  $\text{tr}[\Pi_0 \sigma_{\text{opt}} \Pi_0] + \text{tr}[\Pi_1 \sigma_{\text{opt}} \Pi_1] = 1$ , we obtain

$$R_{\mathbb{F}}(J_{\mathcal{U}_{\mathcal{N}}}) \geq q_0 R_{\mathbb{F}}(\rho_0) + q_1 R_{\mathbb{F}}(\rho_1). \quad (\text{C28})$$

Furthermore, from Eq. (C19) and the convexity of the resource robustness, we obtain

$$R_{\mathbb{F}}(J_{\mathcal{U}_{\mathcal{N}}}) \leq q_0 R_{\mathbb{F}}(\rho_0) + q_1 R_{\mathbb{F}}(\rho_1). \quad (\text{C29})$$

From Eq. (C28) and Eq. (C29), we obtain Eq. (C25).

The optimal state  $\sigma_{\text{opt}} \in \mathbb{F}$  satisfying  $J_{\mathcal{U}_{\mathcal{N}}} \leq R_{\mathbb{F}}(J_{\mathcal{U}_{\mathcal{N}}})\sigma_{\text{opt}}$  can be represented as

$$\sigma_{\text{opt}} = \frac{q_0 R_{\mathbb{F}}(\rho_0) \Pi_0 \sigma_{0,L} \Pi_0 + q_1 R_{\mathbb{F}}(\rho_1) \Pi_1 \sigma_{1,L} \Pi_1}{q_0 R_{\mathbb{F}}(\rho_0) + q_1 R_{\mathbb{F}}(\rho_1)}, \quad (\text{C30})$$

where  $\sigma_{i,L}$  is defined in Eq. (C24). Since this state satisfies the trace-preserving condition  $\text{tr}_{\mathbb{S}}[\sigma_{\text{opt}}] = I/2$ , we obtain

$$R_{\mathbb{Q}}(\mathcal{U}_{\mathcal{N}}) = R_{\mathbb{F}}(J_{\mathcal{U}_{\mathcal{N}}}) = q_0 R_{\mathbb{F}}(\rho_0) + q_1 R_{\mathbb{F}}(\rho_1) \quad (\text{C31})$$

from Eq. (C16) and Eq. (C25).  $\square$

For the fidelity-based measure  $F_{\mathbb{Q}}(\mathcal{U})$ , we have

$$F_{\mathbb{Q}}(\mathcal{U}) = \max_{\mathcal{M} \in \mathbb{Q}} \min_{\rho} F(\mathcal{I} \otimes \mathcal{U}(\rho), \mathcal{I} \otimes \mathcal{M}(\rho)) \quad (\text{C32})$$

$$\leq \max_{\mathcal{M} \in \mathbb{Q}} F(J_{\mathcal{U}}, J_{\mathcal{M}}) \quad (\text{C33})$$

$$= \max_{\mathcal{M} \in \mathbb{Q}} \text{tr}[(\Pi_0 \rho_L(\theta) \Pi_0)(\Pi_0 J_{\mathcal{M}} \Pi_0)] \quad (\text{C34})$$

$$\leq \max_{\sigma \in \mathbb{F}} \text{tr}[\rho(\theta) \sigma] \quad (\text{C35})$$

$$= \frac{1 + \cos \theta}{2}. \quad (\text{C36})$$

Here,  $\Pi_0 = \frac{1}{2}(II + ZZ)$  is the projector onto the eigenspace of  $ZZ$  with eigenvalue  $+1$ ,  $\rho_L(\theta) = \frac{1}{2}(II + \cos \theta XX + \sin \theta YY)$ , and  $\rho(\theta) = \frac{1}{2}(I + \cos \theta X + \sin \theta Y)$ .

Eq. (C32) is the definition of the fidelity-based measure  $F_{\mathbb{Q}}(\mathcal{U})$ . In Eq. (C33), we set  $\rho = |\Psi\rangle\langle\Psi|$ . Eq. (C34) can be obtained from a simple calculation, and we use Eq. (C2) and the fact that the maximum is achieved when  $\Pi_0 J_{\mathcal{M}} \Pi_0 = J_{\mathcal{M}}$  to derive Eq. (C35). Finally, Eq. (C36) is obtained because the maximum is achieved for  $\sigma = \frac{1}{2}(I + X)$ .

By combining Lemma 1, Lemma 2, and Eq. (C36), we obtain the following theorem.

**Theorem 6.** (Restatement of Theorem 5) *Let  $\mathcal{U}(\cdot) = e^{-i\frac{\theta}{2}Z} \cdot e^{i\frac{\theta}{2}Z}$  be a Pauli-Z rotation gate with  $0 \leq \theta \leq \pi/4$ , and let  $\mathcal{U}_{\mathcal{N}} = \mathcal{N} \circ \mathcal{U}$  be a noisy channel affected by single-qubit Pauli noise  $\mathcal{N}(\cdot) = p_0 \cdot + p_x X \cdot X + p_y Y \cdot Y + p_z Z \cdot Z$ . Then, the worst-case fidelity between the ideal channel  $\mathcal{U}$  and the purified noisy channel  $\Theta(\mathcal{U}_{\mathcal{N}})$  under a stabilizer-preserving superchannel  $\Theta \in \mathbb{S}$  is upper bounded as*

$$F(\Theta(\mathcal{U}_{\mathcal{N}}), \mathcal{U}) \leq \frac{1 + \cos \theta}{2} \left( (p_0 + p_z) R\left(\theta, \frac{p_z}{p_0 + p_z}\right) + (p_x + p_y) R\left(\theta, \frac{p_y}{p_x + p_y}\right) \right), \quad (\text{C37})$$

$$F(\Theta(\mathcal{U}_{\mathcal{N}}), \mathcal{U}) \leq 1 - \frac{1 - \cos \theta}{2} \left( (p_0 + p_z) W\left(\theta, \frac{p_z}{p_0 + p_z}\right) + (p_x + p_y) W\left(\theta, \frac{p_y}{p_x + p_y}\right) \right). \quad (\text{C38})$$

Here,  $R(\theta, p)$  and  $W(\theta, p)$  are defined in Eq. (C14) and Eq. (C15).

Notably, for  $\theta = \pi/4$  and assuming  $\frac{p_z}{p_0 + p_z}, \frac{p_y}{p_x + p_y} < \frac{2 - \sqrt{2}}{4}$ , the two bound simplifies to the same bound of

$$F(\Theta^{\text{cor}}(\mathcal{U}_{\mathcal{N}}), \mathcal{U}) \leq 1 - p_y - p_z, \quad (\text{C39})$$

which can be saturated by SCV under Pauli symmetry. While the original bounds are based on two distinct resource measures, which are resource robustness and resource weight, they boil down to the same inequality. This may suggest an as yet unexplored relationship between the two resource measures. Moreover, while the original bound in Ref. [38] (Lemma 1 in our manuscript) applies to axiomatically defined superchannels  $\Theta \in \mathbb{S}$  in Eq. (C4)—which is much larger than the set of operationally motivated superchannels  $\Theta_{\text{Cliff}}^{\text{cor}}$  and thus was expected to only give loose bounds for practical settings—the bound can, in fact, be achieved using our operational protocols. This result not only demonstrates the effectiveness of SCV but also provides theoretical insights into dynamical resource theories by establishing the tightness and practical significance of this general bound.

[1] P. W. Shor, Scheme for reducing decoherence in quantum computer memory, *Phys. Rev. A* **52**, R2493 (1995).

[2] E. Knill, R. Laflamme, and W. Zurek, Threshold accu-

- racy for quantum computation, [arXiv:quant-ph/9610011](https://arxiv.org/abs/quant-ph/9610011) (1996).
- [3] D. Aharonov and M. Ben-Or, Fault-tolerant quantum computation with constant error, in *Proc. 29th Annu. ACM Symp. Theory Comput.* (1997) pp. 176–188.
  - [4] D. A. Lidar and T. A. Brun, *Quantum error correction* (Cambridge university press, 2013).
  - [5] N. Ofek, A. Petrenko, R. Heeres, P. Reinhold, Z. Leghtas, B. Vlastakis, Y. Liu, L. Frunzio, S. Girvin, L. Jiang, *et al.*, Extending the lifetime of a quantum bit with error correction in superconducting circuits, *Nature* **536**, 441 (2016).
  - [6] S. Krinner, N. Lacroix, A. Remm, A. Di Paolo, E. Genois, C. Leroux, C. Hellings, S. Lazar, F. Swiadek, J. Herrmann, *et al.*, Realizing repeated quantum error correction in a distance-three surface code, *Nature* **605**, 669 (2022).
  - [7] Google Quantum AI, Suppressing quantum errors by scaling a surface code logical qubit, *Nature* **614**, 676 (2023).
  - [8] V. Sivak, A. Eickbusch, B. Royer, S. Singh, I. Tsioutsios, S. Ganjam, A. Miano, B. Brock, A. Ding, L. Frunzio, *et al.*, Real-time quantum error correction beyond break-even, *Nature* **616**, 50 (2023).
  - [9] D. Bluvstein, S. J. Evered, A. A. Geim, S. H. Li, H. Zhou, T. Manovitz, S. Ebadi, M. Cain, M. Kalinowski, D. Hangleiter, *et al.*, Logical quantum processor based on reconfigurable atom arrays, *Nature* **626**, 58 (2024).
  - [10] Google Quantum AI and Collaborators, Quantum error correction below the surface code threshold, *Nature* **638**, 920 (2024).
  - [11] K. Temme, S. Bravyi, and J. M. Gambetta, Error mitigation for short-depth quantum circuits, *Phys. Rev. Lett.* **119**, 180509 (2017).
  - [12] S. Endo, Z. Cai, S. C. Benjamin, and X. Yuan, Hybrid quantum-classical algorithms and quantum error mitigation, *J. Phys. Soc. Japan* **90**, 032001 (2021).
  - [13] Z. Cai, R. Babbush, S. C. Benjamin, S. Endo, W. J. Huggins, Y. Li, J. R. McClean, and T. E. O’Brien, Quantum error mitigation, *Rev. Mod. Phys.* **95**, 045005 (2023).
  - [14] Y. Kim, A. Eddins, S. Anand, K. X. Wei, E. Van Den Berg, S. Rosenblatt, H. Nayfeh, Y. Wu, M. Zaletel, K. Temme, *et al.*, Evidence for the utility of quantum computing before fault tolerance, *Nature* **618**, 500 (2023).
  - [15] X. Bonet-Monroig, R. Sagastizabal, M. Singh, and T. E. O’Brien, Low-cost error mitigation by symmetry verification, *Phys. Rev. A* **98**, 062339 (2018).
  - [16] S. McArdle, X. Yuan, and S. Benjamin, Error-mitigated digital quantum simulation, *Phys. Rev. Lett.* **122**, 180501 (2019).
  - [17] G. Lee, C. T. Hann, S. Puri, S. M. Girvin, and L. Jiang, Error suppression for arbitrary-size black box quantum operations, *Phys. Rev. Lett.* **131**, 190601 (2023).
  - [18] J. Miguel-Ramiro, Z. Shi, L. Dellantonio, A. Chan, C. A. Muschik, and W. Dür, Superposed quantum error mitigation, *Phys. Rev. Lett.* **131**, 230601 (2023).
  - [19] Z. Liu, X. Zhang, Y.-Y. Fei, and Z. Cai, Virtual channel purification, [arXiv:2402.07866](https://arxiv.org/abs/2402.07866) (2024).
  - [20] Y. Xiong, D. Chandra, S. X. Ng, and L. Hanzo, Circuit symmetry verification mitigates quantum-domain impairments, *IEEE Trans. Signal Process.* **71**, 477 (2023).
  - [21] D. M. Debroy and K. R. Brown, Extended flag gadgets for low-overhead circuit verification, *Phys. Rev. A* **102**, 052409 (2020).
  - [22] A. Gonzales, R. Shaydulin, Z. H. Saleem, and M. Suchara, Quantum error mitigation by pauli check sandwiching, *Sci. Rep.* **13**, 2122 (2023).
  - [23] E. van den Berg, S. Bravyi, J. M. Gambetta, P. Jurcevic, D. Maslov, and K. Temme, Single-shot error mitigation by coherent pauli checks, *Phys. Rev. Res.* **5**, 033193 (2023).
  - [24] S. Das, J. Sun, M. Hanks, B. Koczor, and M. Kim, Purification and correction of quantum channels by commutation-derived quantum filters, [arXiv:2407.20173](https://arxiv.org/abs/2407.20173) <https://doi.org/10.48550/arXiv.2407.20173> (2024).
  - [25] N. Yoshioka, S. Akibue, H. Morisaki, K. Tsubouchi, and Y. Suzuki, Error crafting in mixed quantum gate synthesis, [arXiv:2405.15565](https://arxiv.org/abs/2405.15565) (2024).
  - [26] J. R. McClean, Z. Jiang, N. C. Rubin, R. Babbush, and H. Neven, Decoding quantum errors with subspace expansions, *Nat. Commun.* **11**, 636 (2020).
  - [27] Z. Cai, Quantum error mitigation using symmetry expansion, *Quantum* **5**, 548 (2021).
  - [28] S. Endo, Y. Suzuki, K. Tsubouchi, R. Asaoka, K. Yamamoto, Y. Matsuzaki, and Y. Tokunaga, Quantum error mitigation for rotation symmetric bosonic codes with symmetry expansion, [arXiv:2211.06164](https://arxiv.org/abs/2211.06164) (2022).
  - [29] K. Tsubouchi, Y. Suzuki, Y. Tokunaga, N. Yoshioka, and S. Endo, Virtual quantum error detection, *Phys. Rev. A* **108**, 042426 (2023).
  - [30] G. H. Low and I. L. Chuang, Optimal hamiltonian simulation by quantum signal processing, *Phys. Rev. Lett.* **118**, 010501 (2017).
  - [31] R. Babbush, C. Gidney, D. W. Berry, N. Wiebe, J. McClean, A. Paler, A. Fowler, and H. Neven, Encoding electronic spectra in quantum circuits with linear t complexity, *Phys. Rev. X* **8**, 041015 (2018).
  - [32] G. H. Low and I. L. Chuang, Hamiltonian simulation by qubitization, *Quantum* **3**, 163 (2019).
  - [33] N. Yoshioka, T. Okubo, Y. Suzuki, Y. Koizumi, and W. Mizukami, Hunting for quantum-classical crossover in condensed matter problems, *npj Quantum Inf.* **10**, 45 (2024).
  - [34] C. Piveteau, D. Sutter, S. Bravyi, J. M. Gambetta, and K. Temme, Error mitigation for universal gates on encoded qubits, *Phys. Rev. Lett.* **127**, 200505 (2021).
  - [35] M. Lostaglio and A. Ciani, Error mitigation and quantum-assisted simulation in the error corrected regime, *Phys. Rev. Lett.* **127**, 200506 (2021).
  - [36] Y. Suzuki, S. Endo, K. Fujii, and Y. Tokunaga, Quantum error mitigation as a universal error reduction technique: Applications from the nisq to the fault-tolerant quantum computing eras, *PRX Quantum* **3**, 010345 (2022).
  - [37] K. Tsubouchi, Y. Mitsushashi, K. Sharma, and N. Yoshioka, Symmetric clifford twirling for cost-optimal quantum error mitigation in early ftqc regime, [arXiv:2405.07720](https://arxiv.org/abs/2405.07720) (2024).
  - [38] B. Regula and R. Takagi, Fundamental limitations on distillation of quantum channel resources, *Nat. Commun.* **12**, 4411 (2021).
  - [39] K. Tsubouchi, T. Sagawa, and N. Yoshioka, Universal cost bound of quantum error mitigation based on quantum estimation theory, *Phys. Rev. Lett.* **131**, 210601 (2023).
  - [40] R. Takagi, H. Tajima, and M. Gu, Universal sampling lower bounds for quantum error mitigation, *Phys. Rev. Lett.* **131**, 210602 (2023).

- [41] R. Takagi, S. Endo, S. Minagawa, and M. Gu, Fundamental limits of quantum error mitigation, *npj Quantum Inf.* **8**, 114 (2022).
- [42] Y. Quek, D. Stilck França, S. Khatri, J. J. Meyer, and J. Eisert, Exponentially tighter bounds on limitations of quantum error mitigation, *Nat. Phys.* **20**, 1648 (2024).
- [43] B. Peng, S. Gulania, Y. Alexeev, and N. Govind, Quantum time dynamics employing the yang-baxter equation for circuit compression, *Phys. Rev. A* **106**, 012412 (2022).
- [44] E. Rosenberg, T. Andersen, R. Samajdar, A. Petukhov, J. Hoke, D. Abanin, A. Bengtsson, I. Drozdov, C. Erickson, P. Klimov, *et al.*, Dynamics of magnetization at infinite temperature in a heisenberg spin chain, *Science* **384**, 48 (2024).
- [45] N. J. Ross and P. Selinger, Optimal ancilla-free clifford+t approximation of z-rotations., *Quantum Inf. Comput.* **16**, 901 (2016).
- [46] T. Oka and S. Kitamura, Floquet engineering of quantum materials, *Annu. Rev. Condens. Matter Phys.* **10**, 387 (2019).
- [47] X. Mi, M. Ippoliti, C. Quintana, A. Greene, Z. Chen, J. Gross, F. Arute, K. Arya, J. Atalaya, R. Babbush, *et al.*, Time-crystalline eigenstate order on a quantum processor, *Nature* **601**, 531 (2022).
- [48] P. Frey and S. Rachel, Realization of a discrete time crystal on 57 qubits of a quantum computer, *Sci. Adv.* **8**, eabm7652 (2022).
- [49] M. Ippoliti, K. Kechedzhi, R. Moessner, S. Sondhi, and V. Khemani, Many-body physics in the nisq era: Quantum programming a discrete time crystal, *PRX Quantum* **2**, 030346 (2021).
- [50] A. G. Fowler, Constructing arbitrary steane code single logical qubit fault-tolerant gates, *Quantum Inf. Comput.* **11**, 867 (2011).
- [51] A. Bocharov and K. M. Svore, Resource-optimal single-qubit quantum circuits, *Phys. Rev. Lett.* **109**, 190501 (2012).
- [52] J. Emerson, R. Alicki, and K. Życzkowski, Scalable noise estimation with random unitary operators, *J. Opt. B: Quantum Semiclass. Opt.* **7**, S347 (2005).
- [53] C. Dankert, R. Cleve, J. Emerson, and E. Livine, Exact and approximate unitary 2-designs and their application to fidelity estimation, *Phys. Rev. A* **80**, 012304 (2009).
- [54] A. Dutkiewicz, S. Polla, M. Scheurer, C. Gogolin, W. J. Huggins, and T. E. O'Brien, Error mitigation and circuit division for early fault-tolerant quantum phase estimation, *arXiv:2410.05369* (2024).
- [55] M. A. Nielsen and I. L. Chuang, *Quantum computation and quantum information* (Cambridge university press, 2010).
- [56] D. Gottesman, *Surviving as a quantum computer in a classical world* (Textbook manuscript preprint, 2024).
- [57] Z. Jiang, J. McClean, R. Babbush, and H. Neven, Majorana loop stabilizer codes for error mitigation in fermionic quantum simulations, *Phys. Rev. Appl.* **12**, 064041 (2019).
- [58] S. Zhou, Z.-W. Liu, and L. Jiang, New perspectives on covariant quantum error correction, *Quantum* **5**, 521 (2021).
- [59] A. Kubica and R. Demkowicz-Dobrzański, Using quantum metrological bounds in quantum error correction: A simple proof of the approximate eastin-knill theorem, *Phys. Rev. Lett.* **126**, 150503 (2021).
- [60] S. Zhou, M. Zhang, J. Preskill, and L. Jiang, Achieving the heisenberg limit in quantum metrology using quantum error correction, *Nat. Commun.* **9**, 78 (2018).
- [61] G. Vidal and R. Tarrach, Robustness of entanglement, *Phys. Rev. A* **59**, 141 (1999).
- [62] F. G. S. L. Brandão and G. Gour, Reversible framework for quantum resource theories, *Phys. Rev. Lett.* **115**, 070503 (2015).
- [63] R. Takagi and B. Regula, General resource theories in quantum mechanics and beyond: Operational characterization via discrimination tasks, *Phys. Rev. X* **9**, 031053 (2019).
- [64] J. R. Seddon and E. T. Campbell, Quantifying magic for multi-qubit operations, *Proc. R. Soc. A* **475**, 20190251 (2019).
- [65] G. Brassard, P. Hoyer, M. Mosca, and A. Tapp, Quantum amplitude amplification and estimation, *quant-ph/0005055* (2000).
- [66] M. J. Bremner, R. Jozsa, and D. J. Shepherd, Classical simulation of commuting quantum computations implies collapse of the polynomial hierarchy, *Proc. R. Soc. A-Math. Phys. Eng. Sci.* **467**, 459 (2011).
- [67] M. J. Bremner, A. Montanaro, and D. J. Shepherd, Average-case complexity versus approximate simulation of commuting quantum computations, *Phys. Rev. Lett.* **117**, 080501 (2016).
- [68] F. Zhou, J. Williams, S. Sun, C. D. Malliakas, M. G. Kanatzidis, A. F. Kemper, and C.-Y. Ruan, Nonequilibrium dynamics of spontaneous symmetry breaking into a hidden state of charge-density wave, *Nat. Commun.* **12**, 566 (2021).
- [69] O. Hahn, G. Ferrini, and R. Takagi, Bridging magic and non-gaussian resources via gottesman-kitaev-preskill encoding, *PRX Quantum* **6**, 010330 (2025).
- [70] R. Chao and B. W. Reichardt, Flag fault-tolerant error correction for any stabilizer code, *PRX Quantum* **1**, 010302 (2020).
- [71] Y. Mitsuhashi and N. Yoshioka, Clifford group and unitary designs under symmetry, *PRX Quantum* **4**, 040331 (2023).
- [72] C. Gidney, Halving the cost of quantum addition, *Quantum* **2**, 74 (2018).
- [73] K. Fang and Z.-W. Liu, No-go theorems for quantum resource purification: New approach and channel theory, *PRX Quantum* **3**, 010337 (2022).
- [74] V. Veitch, S. A. Hamed Mousavian, D. Gottesman, and J. Emerson, The resource theory of stabilizer quantum computation, *New J. Phys.* **16**, 013009 (2014).
- [75] G. Chiribella, G. M. D'Ariano, and P. Perinotti, Transforming quantum operations: Quantum supermaps, *Europhysics Letters* **83**, 30004 (2008).
- [76] G. Chiribella, G. M. D'Ariano, and P. Perinotti, Quantum circuit architecture, *Phys. Rev. Lett.* **101**, 060401 (2008).
- [77] M. Lewenstein and A. Sanpera, Separability and entanglement of composite quantum systems, *Phys. Rev. Lett.* **80**, 2261 (1998).
- [78] R. Uola, T. Bullock, T. Kraft, J.-P. Pellonpää, and N. Brunner, All quantum resources provide an advantage in exclusion tasks, *Phys. Rev. Lett.* **125**, 110402 (2020).
- [79] M. G. Díaz, K. Fang, X. Wang, M. Rosati, M. Skotiniotis, J. Calsamiglia, and A. Winter, Using and reusing coherence to realize quantum processes, *Quantum* **2**, 100 (2018).



[80] R. Rubboli, R. Takagi, and M. Tomamichel, Mixed-state additivity properties of magic monotones based on quan-

tum relative entropies for single-qubit states and beyond, *Quantum* **8**, 1492 (2024).